Analysis of Elastic Wave Propagation Through Thin Shell Modelled Flexible Pipes
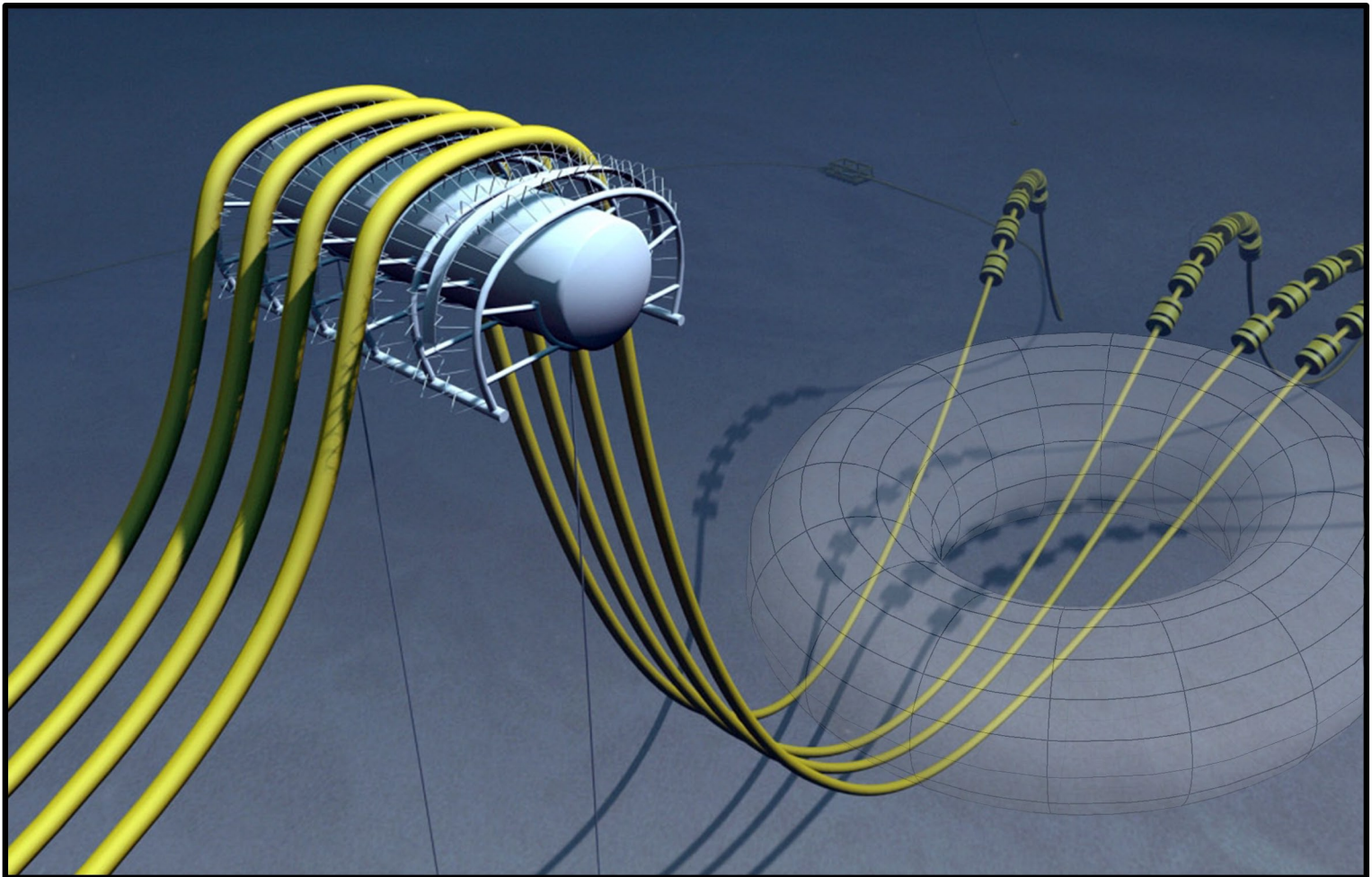
Master's Thesis by Jonas Morsbøl
Spring 2011

Design of Mechanical Systems
Department of Mechanical &Manufacturing Engineering

AALBORG UNIVERSITET

Preface

This thesis has been written in a hurry at the end of an interesting tenth semester of the *Design of Mechanical Systems*-program at Aalborg University, spring 2011. The thesis can be regarded as a pre-study for a PhD-project at Aalborg University titled *Advanced Modelling of Wave Propagation in Curved Elastic Fluid-Loaded Pipes.* The PhD-project is supposed to be launched in the autumn 2011. The PhD-stipend is funded by *The Danish Council for Independent Research | Technology and Production Sciences* (FTP) and supported by *NKT Flexibles I/S* through possible empirical data and gives the project an immediate industrial relevance. Both the PhD-project and this thesis are supervised by Prof. Sergey V. Sorokin while Development Engineer Anders Lyckegaard is the contact person to NKT Flexibles.

At the launch of this semester the ambition where to establish a shell model of a thin walled toroidal shell. This model should represent a curved segment of a flexible pipe. From this model the dynamical properties of such geometry should be extracted. Already from the beginning it where expected that this shell model would contain quiet cumbersome equations. It would then be relevant to approximate the results of the model through asymptotic analysis and perturbation methods. In the mean time the development and benchmarking of the toroidal shell model turned out to be more time demanding than expected. And as long as the reliability of the shell model is unclear it has not been found relevant to proceed to next step and approximate the model by means of perturbation.

Figures and equations are numbered according to the chapter in which they are presented—for instance: *figure 1.2* is the 2nd figure in chapter 1. Appendices are labelled with capital letters followed by a section number—for instance: *A.1* is the 1st section in appendix A. Citations and references are done in accordance with the Harvard Style where the name of the author and year of publication are given in square brackets. The bibliography is found on page 43. If not anything else is stated then the following mathematical notation is used throughout the text:

Scalar: a
Vector: $\mathbf{a}$
Matrix: $\mathbf{A}$

<div style="text-align:center">

_____

Jonas Morsbøl

</div>

Contents

Abstract

Flexible pipes are used in the oil and gas industry to transport various kinds of fossil fluid. One application is to use a pipe as a riser, transporting crude oil or natural gas from the seabed to an oil rig or a tank ship hovering in surface of the sea. A common issue with these kinds of pipes is generation of vibrations due to the fluid flowing inside. These vibrations can be transmitted through the pipe as elastic waves potentially resulting in fatigue failure of the components attached to the ends of the pipe. With the aim of reducing these vibrations at the ends, a study of the waveguide properties of such pipes is needed. The first step in this study is, in this thesis, taken by investigating the wave guide properties of a infinite toroidal shell. The waveguide properties of an infinite toroidal shell can later be used to determine the wave guide properties of a small section of the torus by means of boundary integral equations method. The small section of the torus can be thought of as representing a bend thin walled pipe section. It has been chosen to model the pipe as a shell in order take the flexibility of the cross section into account. The toroidal shell model has been benchmarked against, respectively, classical Bernoulli-Euler beam theory and curved beam theory. The first comparison is relevant when the radius of the torus is very large. Due to same reason a shell model of a thin walled cylinder has also been established and benchmarked against the toroidal shell. The benchmarking is made between dispersion curves for some of the simplest vibration modes covered by both theories. The dispersion curves are obtained by enforcing a trial solution on the differential equations governing the system and a system of equally many equations and unknowns is obtained by imposing Galerkin's method. Different trial solutions representing, respectively, in-plane bending and out-off-plane bending, have been enforced on the toroidal shell model in fashion of truncated complex Fourier series and the converge of the dispersion curves related to some of the simplest vibrations modes has been studied. From these studies it can be concluded that the governing differential equations of the toroidal shell, which have been derived, are valid.

Chapter

1

Introduction

Flexible pipes are used in the oil and gas industry to transport various kinds of fossil fluid. One application is to use a pipe as a riser, transporting crude oil or natural gas from the seabed to an oil rig or a tank ship hovering in surface of the sea. Such situation is illustrated in figure 1.1. One of the demands for this application is that the local strength of the pipe is sufficiently high to withstand the pressure difference between the fluid inside the pipe and the surrounding seawater. But at same time the pipes must be globally flexible to let the ship or the oil rig follow the vertical movements due to the waves on the surface of the sea. Such demands can be met by founding the pipe design on a corrugated steel pipe. Figure 1.2 shows a profile of such pipe.
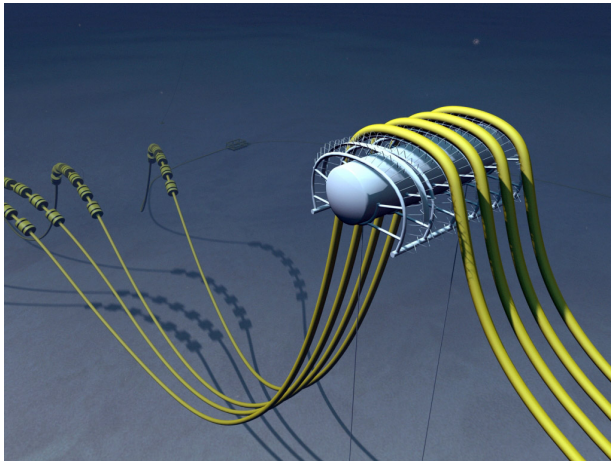
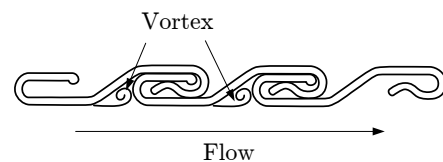**Figure 1.1:** *A typical situation where the risers hovering in the seawater (From: NKT Flexibles)*

Figure 1.2: *The inner wall of a corrugated pipe. (From: Goyder [2009])*

As illustrated in the figure, when fluid is flowing inside the pipe, vortexes can be generated at the inner pipe wall due to the cavities of the corrugation. It is common that these vortexes induce time varying forcing of the pipe wall, cf. Nakiboglu [2010]. The time varying forcing can then be transferred as elastic waves travelling through the pipe. Elastic waves travelling through the pipe can also be induced if the pipe is attached to oscillating machinery at the seabed. Time varying forcing is the driving force with respect to crack initiation, crack growth, and fatigue in general. Due to the high safety demands in the oil and gas industry the encouragement for predicting and possibly reducing such fatigue inducing mechanisms is obvious.

NKT Flexibles is a Danish company specialised in designing and producing this kind of pipes. Their experience is not that these vibrations are fatiguing the pipe, leading to leakage of the pipe itself. Their concern is rather the possibility of fatigue failure of the components mounted to each end of the pipe – i.e. end fittings and the piping system followed by the

mounting points. Thus NKT Flexibles are interested in how vibrations are transmitted from the source to the pipe ends. With a goal of reducing the wave transmission, a deeper understanding of how waves are transmitted through the pipes can yield more well-founded suggestions for design changes. Knowledge about wave transmission also facilitates the ability of predicting the vibrational output at the pipe end due to a vibrational excitation along, or at the other end, of the pipe. An ambitious utilisation of such prediction is to monitor the vibrations at appropriate locations along the pipe. Then, during the transmission time of the waves, the signals from the monitoring can be processed in order to produce a proper counter respond when the waves arrive at the end of the pipe.

These considerations point in direction of an analytical approach. A by-product of an analytical approach is a direct insight into the intermediate results. And because a valid analytical model typically only incorporates the most important mechanisms, which are governing the system, an insight into the intermediate results can enhance the understanding of how these mechanisms affect the final result. Evaluation of an analytical model is often also very time efficient. This is indeed needed if the ambition of actively damping the vibrations, by monitoring along the pipe, is to be realised. Thus an analytical approach is not only academically appealing but is also highly industrial relevant.

Figure 1.3: *The picture show the different layers of a NKT Flexibles pipe. (From: NKT Flexibles)*

Figure 1.3 illustrates the complexity of a typical pipe produced by NKT Flexibles. The different layers consist of the corrugated inner pipe and a series of polymer layer, sealing the pipe, and steel armour adding strength to the pipe. The steel armour is oriented in different directions adding strength in the axial direction of the pipe and in the circumferential direction of the pipe. Due to these complications a thorough analysis of the dynamical properties of the structure itself, is a demanding task. In addition to this the possible interactions between the structure and the fluid inside and outside the pipe must be taken into account in order to obtain a reliable prediction of the wave guide properties in its working environment. This also makes the analysis multidisciplinary.

1.1 Thesis Outline and Essential Limitations

A long-termed objective is naturally to gain sufficient knowledge to predict the wave guide properties of a pipe having all the complications as described just above. But instead of simply launching the project by stating this objective it is found convenient to break down the analysis into delimited subtasks. An essential property of any flexible pipe, suitable for the above

described application, is that it can be regarded as an initially straight pipe. Though during its application, it is hovering in the water column of the sea in an irregular configuration of primarily slightly bend sections. Due to this essentiality the first milestone will be to investigate the influence of introducing a bend on a generally flexible pipe. Thus the impact of introducing a bend is expected to be relevant regardless the specific design of the wall of the flexible pipe.

With the aim of solely investigate the effects of the bending, the pipe will in this thesis be regarded as isotropic, homogeneous, and single layered. Along with this only one bend, having a constant bending radius, will be studied. The flexibility of the pipe will be attained by modelling the pipe as a thin walled shell. Compared to conventional beam theory this adds extra degrees of freedom to the cross section of the pipe, making it possible to attain circumferential vibration modes which cannot be obtained by beam theory. On the other hand the shell model will still be able to attain all modes covered by the beam theory. Thus the beam theory can be used in benchmarking of the shell model.

The geometry of a thin walled flexible pipe, forming a single bend with a constant bending radius, can be thought of as a section of a torus. It is possible to mathematically parameterise such geometry and thus the foundation for an analytical shell model exists. In the mean time it is convenient first to study the wave guide properties of free vibrations in an unbounded geometry and then later enforce the conditions at the boundaries by means of *Boundary Integral Equations Method*, cf. Sorokin [2010]. An unbounded torus can be thought of as an infinite cylinder which has been bend into a torus overlapping itself in an infinite number of times. Thus the torus cannot in this case be thought of as a closed ring, but is rather an abstract geometry. Determination of the wave guide properties in an infinite toroidal shell is in itself a challenging task. But when it is accomplished it defines the backbone of the analysis of wave propagation in flexible pipes of finite length. In this thesis the wave guide properties of free vibrations in the infinite geometry will be studied.

1.2 Approach of Modelling

Besides employing an analytical approach, the following subjects will be examined and discussed throughout the thesis in order to develop and benchmark the toroidal shell model:

- As a point of reference a shell model of a thin walled infinite cylinder will be established. From this model the so-called *dispersion curves* will be determined. The dispersion curves are essential for the dynamical properties of a geometry and they hold the relation between the wave number, characterising the wave propagation, and the frequency.

- The cylinder model will be benchmarked against classical Bernoulli-Euler beam theory by means of these dispersion curves for some of the simplest free vibrational modes for the geometry.

- When the cylinder shell has been modelled and verified through classical beam theory the modelling advances with the development of a toroidal shell model. Also here the dispersion curves will be extracted. As will be demonstrated these dispersion curves are at first hand used to tune in the shell model in order to obtain converged results.

- The dispersion curves from the toroidal shell model will be benchmarked against curved beam theory, again for some of the simplest vibrational modes. Subsequently the dispersion curves of the toroidal shell model will be compared to the corresponding curves of the cylinder model. When the torus is straightened out it approaches the geometry of the cylinder and thus their properties must coincide at the limit.

Initially the ambition for this thesis where to proceed with asymptotic expansion of the relation between the wave number and the frequency by means of perturbation methods. But as explained in the preface the modelling, benchmarking, and tuning of the torus model turned out to be more time consuming than expected, and thereby it where found irrelevant to produce asymptotic expansion before the validity of the analytical model were ensured.

With these introducing considerations the thesis will start with a short review of the general thin shell theory.

Chapter

2

Thin Shell Theory

In this chapter some important relations from the general theory of thin shells will be presented. The relations along with their fundamental assumptions will be presented and briefly discussed in accordance with Novozhilov [1959] while the thorough derivations leading to these relations are omitted.

2.1   Initial Definitions and Assumptions

A shell can be characterised as a continuum bounded by two closely spaced and smooth surfaces where the distance between the two surfaces can be regarded as the thickness of the shell. The fact the two bounding surfaces must be closely spaced and smooth implies that the thickness of the shell is small compared to the other dimensions of the shell, but it do not necessarily requires the thickness to be constant throughout the shell. The middle of the distance between the two surfaces bounding the shell defines the so-called *middle surface*. This is analogue to the centre line of the beam in classical Bernoulli-Euler beam theory. Like in the beam theory, where the deformation of any point in the beam is determined from the displacement of the centre line, the deformation of any point in the shell is determined from the displacement of the middle surface. Thus, the main concern in the shell theory is the displacement of the middle surface from its un-deformed configuration. Returning to the definition of the shell the term *small* was used to characterise the thickness of the shell. To give a more precise quantification of this smallness it is stated by Novozhilov that within the present thin shell theory a relative error of less than 5 % is obtained if the following inequality, at any point of the shell, is not violated:

$$\frac{h}{R} \leq \frac{1}{20} \tag{2.1}$$

where: h Thickness of the shell at a given location.

          R Smallest radius of curvature of the middle surface at the same given location.

If this inequality is violated the shell cannot be regarded as a thin shell and the relative error if applying the present theory can then be more than 5 %.

2.2 Basic Results of Elementary Differential Geometry

A prerequisite in determining the displacement of the middle surface of the shell is a mathematical description of the un-deformed configuration of the middle surface. This mathematical description can be based on a two-dimensional mesh wrapping the middle surface. This is illustrated in figure 2.1. Thus the mathematical description can be grasped as a mapping
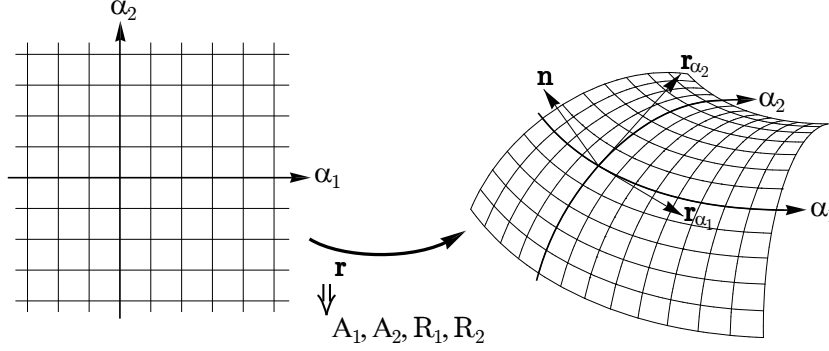

Figure 2.1: *The mapping from the two-dimensional Cartesian coordinate system to the curved surface of the shell is controlled by the parameters A_1, A_2, R_1, and R_2.*

from a two-dimensional mesh to a three-dimensional generally curved surface. As illustrated in the figure, any point in the two-dimensional mesh can be determined by the coordinates α_1 and α_2, also called *curvilinear coordinates*. Based on these two coordinates the mapping to the curved surface can be formulated as a parameterisation of the following form:

$$\mathbf{r} = \begin{bmatrix} x \\ y \\ z \end{bmatrix} = \begin{bmatrix} f_1(\alpha_1, \alpha_2) \\ f_2(\alpha_1, \alpha_2) \\ f_3(\alpha_1, \alpha_2) \end{bmatrix} \tag{2.2}$$

where: x, y, z Global cartesian coordinates.

From the parametrisation, $\mathbf{r}$, the four parameters A_1, A_2, R_1, and R_2 can be derived. The two first are called *Lamé parameters* whereas the two later expresses the two principal radii of curvature of the shell. In the shell theory they are used to extract information from the parameterisation about the geometry of the middle surface. The Lamé parameters contains information about how the curvilinear coordinates are stretched or compressed when they are mapped on the surface while the radii of curvature naturally contains information about how the they are curved. Because the parameterisation is formulated on the curvilinear coordinates then both the Lamé parameters and the radii of curvature are in general also functions of the curvilinear coordinates. The Lamé parameters are derived from the two partial derivatives of the parameterisation with respect to α_1 and α_2:

$$\mathbf{r}_{\alpha_1} = \frac{\partial \mathbf{r}}{\partial \alpha_1}, \qquad \mathbf{r}_{\alpha_2} = \frac{\partial \mathbf{r}}{\partial \alpha_2} \tag{2.3}$$

The first vector is tangential to the curves generated on the surface, by varying α_1 while keeping α_2 constant. Likewise is the second vector tangential to the curves generated by varying α_2. This is also illustrated in figure 2.1. If α_1 is increased by an infinitesimal step, $d\alpha_1$ then the corresponding path length on the surface, ds_1, is determined from:

$$ds_1 = \left| \frac{\partial \mathbf{r}}{\partial \alpha_1} \right| d\alpha_1 \tag{2.4}$$

where: $|\mathbf{a}|$ Length of vector $\mathbf{a}$.

And equivalently for $d\alpha_2$:

$$ds_2 = \left| \frac{\partial \mathbf{r}}{\partial \alpha_2} \right| d\alpha_2 \tag{2.5}$$

The Lamé parameters are now defined as:

$$A_1(\alpha_1, \alpha_2) \equiv \left| \frac{\partial \mathbf{r}}{\partial \alpha_1} \right| = \sqrt{\left(\frac{\partial x}{\partial \alpha_1} \right)^2 + \left(\frac{\partial y}{\partial \alpha_1} \right)^2 + \left(\frac{\partial z}{\partial \alpha_1} \right)^2}$$

$$A_2(\alpha_1, \alpha_2) \equiv \left| \frac{\partial \mathbf{r}}{\partial \alpha_2} \right| = \sqrt{\left(\frac{\partial x}{\partial \alpha_2} \right)^2 + \left(\frac{\partial y}{\partial \alpha_2} \right)^2 + \left(\frac{\partial z}{\partial \alpha_2} \right)^2}$$

$$\tag{2.6}$$

As mentioned earlier the two parameters, R_1 and R_2, are the two principal radii of curvature of the surface. Along with this it is assumed that the parameterisation is formulated such that the directions of the curves generated on the curved surface, by varying one of the curvilinear coordinates at the time, coincide with the principal directions of the surface. Consequently the curvilinear coordinates are orthogonal when mapped on the surface. Another consequence is that the radii of curvature of these curves also coincide with the principal radii of curvatures of the surface. Naturally the subscripts of respectively the curvilinear coordinates and the radii of curvature are designated such that the radii of curvature of the curves generated by varying α_1 is determined by R_1 and vice versa. The principal radii of curvatures can be determined from a sequence of vector manipulations involving $\mathbf{r}_{\alpha_1}$ and $\mathbf{r}_{\alpha_2}$. A sufficient set of relations making it possible to determine the principal curvatures will here be presented shortly without further discussion. Detailed derivations of these relations can e.g. be found in Raussen [2007].

First six parameters are determined from the so-called *1. fundamental form* and *2. fundamental form*:

1. fundamental form	2. fundamental form
$E(\alpha_1, \alpha_2) = \mathbf{r}_{\alpha_1} \cdot \mathbf{r}_{\alpha_1}$	$e(\alpha_1, \alpha_2) = \frac{\mathbf{r}_{\alpha_1} \times \mathbf{r}_{\alpha_2}}{|\mathbf{r}_{\alpha_1} \times \mathbf{r}_{\alpha_2}|} \cdot \mathbf{r}_{\alpha_1, \alpha_1}$
$F(\alpha_1, \alpha_2) = \mathbf{r}_{\alpha_1} \cdot \mathbf{r}_{\alpha_2}$	$f(\alpha_1, \alpha_2) = \frac{\mathbf{r}_{\alpha_1} \times \mathbf{r}_{\alpha_2}}{|\mathbf{r}_{\alpha_1} \times \mathbf{r}_{\alpha_2}|} \cdot \mathbf{r}_{\alpha_1, \alpha_2}$
$G(\alpha_1, \alpha_2) = \mathbf{r}_{\alpha_2} \cdot \mathbf{r}_{\alpha_2}$	$g(\alpha_1, \alpha_2) = \frac{\mathbf{r}_{\alpha_1} \times \mathbf{r}_{\alpha_2}}{|\mathbf{r}_{\alpha_1} \times \mathbf{r}_{\alpha_2}|} \cdot \mathbf{r}_{\alpha_2, \alpha_2}$

$$\tag{2.7}$$

These parameters are used to calculate the *Gaussian curvature* and the *mean curvature*:

$$K(\alpha_1, \alpha_2) = \frac{eg - f^2}{EG - F^2}$$

$$H(\alpha_1, \alpha_2) = \frac{eG + gE - 2fF}{2\left(EG - F^2 \right)}$$

$$\tag{2.8}$$

Finally the two principal curvatures are found as:

$$k_1(\alpha_1, \alpha_2) = H + \sqrt{H^2 - K}$$

$$k_2(\alpha_1, \alpha_2) = H - \sqrt{H^2 - K}$$

(2.9)

The radii of curvature is found as the reciprocal of the curvature. It must though be emphasised that Raussen [2007] uses opposite sign convention for the radius of curvature compared to Novozhilov. In Novozhilov's book the centre of the negative curvature is found in the direction of the positive surface normal, i.e. in direction of $\mathbf{n} = \mathbf{r}_{\alpha_1} \times \mathbf{r}_{\alpha_2}$, c.f. figure 2.1. In the above relations the surface normal is though pointing in the direction of what is assumed to be the centre of the positive curvature. To match the above relations to the conventions in Novozhilov's book the radii of curvature are here defined as:

$$R_1(\alpha_1, \alpha_2) \equiv -\frac{1}{k_1}$$

$$R_2(\alpha_1, \alpha_2) \equiv -\frac{1}{k_2}$$

(2.10)

With these definitions of the Lamé parameters and the radii of curvature the shell theory can be specialised to any geometry coved by the initial definitions and assumptions presented in previous section.

As a final remark to this section of elementary differential geometry it is pointed out that certain relations between the Lamé parameters and the radii of curvature must be satisfied in order to ensure that they consistently describe the same surface. The relations are called *the conditions of Codazzi* and *the condition of Gauss*. The conditions of Codazzi are:

$$\frac{\partial}{\partial \alpha_1}\left(\frac{A_2}{R_2}\right) = \frac{1}{R_1}\frac{\partial A_2}{\partial \alpha_1}$$

$$\frac{\partial}{\partial \alpha_2}\left(\frac{A_1}{R_1}\right) = \frac{1}{R_2}\frac{\partial A_1}{\partial \alpha_2}$$

(2.11)

And the condition of Gauss is:

$$\frac{\partial}{\partial \alpha_1}\left(\frac{1}{A_1}\frac{\partial A_2}{\partial \alpha_1}\right) + \frac{\partial}{\partial \alpha_2}\left(\frac{1}{A_2}\frac{\partial A_1}{\partial \alpha_2}\right) = -\frac{A_1 A_2}{R_1 R_2}$$

(2.12)

As indicated these identities can be helpful to test the consistency between the Lamé parameters and the radii of curvature.

2.3 Deformations of the Middle Surface

The determination of deformation of the middle surface of the shell is based on a kinematic assumption similar to one of the well-known Kirchhoff assumptions founding the Bernoulli-Euler beam theory. In this thin shell theory, when determining the deformation of the shell, it is assumed that:

> *Any fictive line normal to the middle surface of the shell remains straight and normal to this surface at any instance during deformation of the shell.*

The consequences of this kinematic assumption are identical to assuming that out of plane shearing forces do not contribute to the deformation of the shell. From the kinematic assumption the relations between displacements of the middle surface and its resulting deformations can be derived. These derivations result in six relations expressing six quantities. All six quantities are necessary in order to determine the complete state of deformation in the vicinity of any point in the middle surface. Physically the quantities express; relative elongation along α_1 and α_2, in-plane shearing, changes of curvature in the direction of α_1 and α_2, and finally the twist of the surface. The displacements of any point in the middle surface are given by u, v, and w, which are the projections of the displacement vector[1] on the local frame defined by $\mathbf{r}_{\alpha_1}$, $\mathbf{r}_{\alpha_2}$, and $\mathbf{n}$, c.f. figure 2.1. Relating to these displacements the relations of deformation are:

$$\varepsilon_1 = \frac{1}{A_1}\frac{\partial u}{\partial \alpha_1} + \frac{1}{A_1 A_2}\frac{\partial A_1}{\partial \alpha_2}v + \frac{1}{R_1}w$$

$$\varepsilon_2 = \frac{1}{A_2}\frac{\partial v}{\partial \alpha_2} + \frac{1}{A_1 A_2}\frac{\partial A_2}{\partial \alpha_1}u + \frac{1}{R_2}w$$

$$\gamma = \frac{A_2}{A_1}\frac{\partial}{\partial \alpha_1}\left(\frac{v}{A_2}\right) + \frac{A_1}{A_2}\frac{\partial}{\partial \alpha_2}\left(\frac{u}{A_1}\right)$$

$$\kappa_1 = -\frac{1}{A_1}\frac{\partial}{\partial \alpha_1}\left(\frac{1}{A_1}\frac{\partial w}{\partial \alpha_1} - \frac{u}{R_1}\right) - \frac{1}{A_1 A_2}\frac{\partial A_1}{\partial \alpha_2}\left(\frac{1}{A_2}\frac{\partial w}{\partial \alpha_2} - \frac{v}{R_2}\right)$$

$$\kappa_2 = -\frac{1}{A_2}\frac{\partial}{\partial \alpha_2}\left(\frac{1}{A_2}\frac{\partial w}{\partial \alpha_2} - \frac{v}{R_2}\right) - \frac{1}{A_1 A_2}\frac{\partial A_2}{\partial \alpha_1}\left(\frac{1}{A_1}\frac{\partial w}{\partial \alpha_1} - \frac{v}{R_1}\right)$$

$$\tau = -\frac{1}{A_1 A_2}\left(\frac{\partial^2 w}{\partial \alpha_1 \partial \alpha_2} - \frac{1}{A_1}\frac{\partial A_1}{\partial \alpha_2}\frac{\partial w}{\partial \alpha_1} - \frac{1}{A_2}\frac{\partial A_2}{\partial \alpha_1}\frac{\partial w}{\partial \alpha_2}\right) +$$
$$+ \frac{1}{R_1}\left(\frac{1}{A_2}\frac{\partial u}{\partial \alpha_2} - \frac{1}{A_1 A_2}\frac{\partial A_1}{\partial \alpha_2}u\right) + \frac{1}{R_2}\left(\frac{1}{A_1}\frac{\partial v}{\partial \alpha_1} - \frac{1}{A_1 A_2}\frac{\partial A_2}{\partial \alpha_1}v\right)$$

(2.13)

where: ε Relative elongation.

        γ In-plane shearing.

        κ Relative change of curvature.

        τ Twist.

If $A_1 = A_2 = 1$ and $R_1 = R_2 = \infty$, which corresponds to a plane shell, the relations reduce to:

---

[1] The displacement vector can be extracted from the vector field connecting the un-deformed and the deformed middle surface and is pointing in direction of the deformed configuration.

$$\varepsilon_1 = \frac{\partial u}{\partial \alpha_1}$$

$$\varepsilon_2 = \frac{\partial v}{\partial \alpha_2}$$

$$\gamma = \frac{\partial v}{\partial \alpha_1} + \frac{\partial u}{\partial \alpha_2}$$

$$\kappa_1 = -\frac{\partial^2 w}{\partial \alpha_1^2}$$

$$\kappa_2 = -\frac{\partial^2 w}{\partial \alpha_2^2}$$

$$\tau = -\frac{\partial^2 w}{\partial \alpha_1 \partial \alpha_2}$$

(2.14)

Here the first three can be recognised as the in-plane components of Cauchy's strain tensor given in engineering strains while the last three are known as fundamental in the plate theory, c.f. Timoshenko [1959].

2.4   Equilibrium on a Shell Element

The equilibrium is obtained by applying Newton's second law on any infinitesimal element of the shell. Such element can by separated from the surrounding shell by cutting perpendicular to the middle surface along the boundaries of the intervals $\alpha_{1_0} \leq \alpha_1 \leq \alpha_{1_0} + d\alpha_1$ and $\alpha_{2_0} \leq \alpha_2 \leq \alpha_{2_0} + d\alpha_2$. The behaviour of this element is determined by the stresses acting through the boundaries of the element along with body forces on the element and any possibly loadings on the surface of the shell. In analogy to previous considerations about the middle surface it is also here convenient to relate the stresses through the boundaries of the element and the loadings on its volume and surface to its middle surface. Thus, the stresses through the boundaries are represented by statically equivalent forces and moments acting on the boundaries of the middles surface of the element. These forces and moments are obtained by integrating the stresses over the area of each boundary of the shell element. But because the side lengths of the element are of infinitesimal size the stresses are assumed constant along the directions of the side lengths and are then only possible to vary through the thickness of the shell element. Thus, to make each resulting force and moment independent of the side length of the boundary, through which it is acting, it is normalised by this side length. The unit of the stress resultants are then force per unit length and moment per unit length. The resultants of the stresses are illustrated in positive direction in figure 2.2 and 2.3 where the forces are found in the first figure and moments are found in the second. The explicit relations between the stresses and their resulting forces and moments are not needed here and are thus not presented, but can be found in the book of Novozhilov [1959]. As can be noticed in figure 2.2 the out of plane forces are included even though they were abandoned in previous section where the deformation of the shell were discussed. But as also mentioned the out of plane shearing forces are only neglected when determining the deformations of the shell.
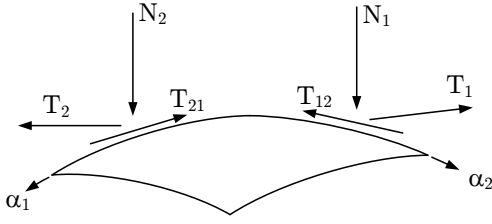
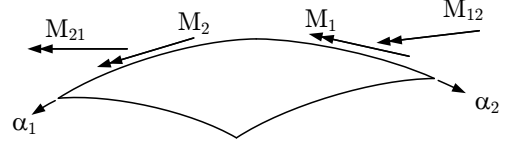**Figure 2.2:** *The positive direction of forces is indicated in the figure. (From: Novozhilov [1959])*

Figure 2.3: *The positive direction of moments is indicated in the figure. (From: Novozhilov [1959])*

Body forces acting on the volume of the shell element and surface tractions acting on the free surfaces are related to the middle surface by considering the smallness of the shell thickness compared to the other dimensions of the shell and by utilising the assumption that the side lengths of the element under consideration are of infinitesimal size. The small shell thickness makes it reasonable to replace the body forces and surface tractions by a statically equivalent forcing distributed over the middle surface without considering the moment arm between the middle surface and the location of the acting point of the actual forcing. Similar it is assumed that due to the infinitesimal side lengths of the element then the statically equivalent forcing distributed over the middle surface is uniform which also means that no moments need to be considered due to body forces or surface tractions. The intensity of the forcing on the middle surface from the body forces and surface tractions can be collected in one quantity which is denominated **q**.

The force equilibrium equations of the shell element are obtained by summing, respectively, all the force differences between the opposite boundaries along with the forcing of the middle surface. This sum is, in accordance with Newton's second law, equated to the time derivative of the linear momentum of the shell element. But following D'Alembert's principle the time derivative of the linear momentum can simply be regarded as a so-called *inertia force* acting as a body force on the element. Thus, any dynamical contribution to the equilibrium can simple be regarded as a part of **q** and the sum of forces are then just equated to zero. At first hand this gives one equilibrium equation in vector form. By projecting this vector equation in the three directions given by the local frame in figure 2.1 the following three differential equations are formed:

$$0 = \frac{1}{A_1 A_2} \left[\frac{\partial (A_2 T_1)}{\partial \alpha_1} + \frac{\partial (A_1 T_{21})}{\partial \alpha_2} + \frac{\partial A_1}{\partial \alpha_2} T_{12} - \frac{\partial A_2}{\partial \alpha_1} T_2 \right] + \frac{N_1}{R_1} + q_1$$

$$0 = \frac{1}{A_1 A_2} \left[\frac{\partial (A_2 T_{12})}{\partial \alpha_1} + \frac{\partial (A_1 T_2)}{\partial \alpha_2} + \frac{\partial A_2}{\partial \alpha_1} T_{21} - \frac{\partial A_1}{\partial \alpha_2} T_1 \right] + \frac{N_2}{R_2} + q_2 \qquad (2.15)$$

$$0 = \frac{1}{A_1 A_2} \left[\frac{\partial (A_2 N_1)}{\partial \alpha_1} + \frac{\partial (A_1 N_2)}{\partial \alpha_2} \right] - \frac{T_1}{R_1} - \frac{T_2}{R_2} + q_n$$

The fact that the inertia force, due to e.g. free vibration of the shell element, can be regarded as a part of **q** makes these equations equally valid for both statics and dynamics.

The moment equilibrium equations are obtained in similar way as the force equilibrium equations by summing all the moment differences between the opposite boundaries. In addition to this the moments created by the shearing forces are also taken into account. The moment due to the forcing of the middle surface is though neglected. This is because it is calculated by multiplying the intensity by the area of the middle surface, $d\alpha_1 d\alpha_2$, and then

crossed by its moment arm which is of same order as $d\alpha_1$ and $d\alpha_2$. This means that the moment due to the forcing of the middle surface is of third order smallness. The moments due to the shearing forces on the boundaries of the element are though calculated by first multiplying the force by the length of the boundary of which it is acting, e.g. $d\alpha_1$, and then by the moment arm, $d\alpha_2$. Thus, these moments are only of second order of smallness, and the moment due to the forcing of the middle surface is then neglected[2]. Like in the derivation of the force equilibrium equations the moments are projected in the directions of the local frame of the shell forming the following three equations:

$$0 = \frac{1}{A_1 A_2} \left[\frac{\partial (A_2 M_1)}{\partial \alpha_1} + \frac{\partial (A_1 M_{21})}{\partial \alpha_2} + \frac{\partial A_1}{\partial \alpha_2} M_{12} - \frac{\partial A_2}{\partial \alpha_1} M_2 \right] - N_1$$

$$0 = \frac{1}{A_1 A_2} \left[\frac{\partial (A_2 M_{12})}{\partial \alpha_1} + \frac{\partial (A_1 M_2)}{\partial \alpha_2} + \frac{\partial A_2}{\partial \alpha_1} M_{21} - \frac{\partial A_1}{\partial \alpha_2} M_1 \right] - N_2 \qquad (2.16)$$

$$0 = T_{12} - T_{21} + \frac{M_{12}}{R_1} - \frac{M_{21}}{R_2}$$

Together with the force equilibrium equations these equations must be obeyed for any such element of the shell. It can in the mean time be shown that the third of moment equilibrium equations is identically satisfied. This can be done by considering that all the terms in this equations are obtained by integrating through the thickness of the shell over the shearing stresses, i.e. σ_{12} or σ_{21}, and imposing the identity that $\sigma_{12} - \sigma_{21} = 0$.

2.5 Strain Energy and the Relations Between Forces and Moments and Deformations

In the previous two sections the relations between displacements and deformations of the middle surface and the equilibrium between forces and moments are given. Here the relations between the forces and moments and the deformation of the middle surface will be given such that the equilibrium between displacements can be established.

The relations between the forces and moments and the deformation of the middle surface takes their origin in the strain energy. To the general expression of strain energy the assumption of out of plane shearing being neglectable is enforced. Along with this, another Kirchhoff assumption is imposed; namely that normal stresses in the direction normal to the middle surface of the shell may also be neglected. Thus, the strain energy can be expressed as:

$$U = \frac{1}{2} \int_V (\sigma_{11}\varepsilon_{11} + \sigma_{22}\varepsilon_{22} + \sigma_{12}\varepsilon_{12}) \, dV \qquad (2.17)$$

where: σ_{ij} Components of Cauchy's stress tensor.

ε_{ij} Components of Cauchy's strain tensor.

V Volume of the shell element.

---

[2]An underlying assumption in these considerations is that the forcing of the middle surface is of maximum same order of magnitude as the shearing forces at the boundaries of the element.

This expression can be rewritten into two different forms. In the first form all stresses are eliminated through Hooke's law and then integrated through the thickness of the shell. Then, if terms of higher order of smallness are cancelled the following can be obtained:

$$U = \frac{Eh}{2\left(1-v^2\right)} \int \int \left((\varepsilon_1 + \varepsilon_2)^2 - 2\left(1-v\right)\left(\varepsilon_1\varepsilon_2 - \frac{\gamma^2}{4}\right)\right) A_1 A_2 d\alpha_1 d\alpha_2 +$$

$$+ \frac{Eh^3}{24\left(1-v^2\right)} \int \int \left((\kappa_1 + \kappa_2)^2 - 2\left(1-v\right)\left(\kappa_1\kappa_2 - \tau^2\right)\right) A_1 A_2 d\alpha_1 d\alpha_2 \qquad (2.18)$$

where: E Young's modulus.

         v Poisson's ratio.

         h Thickness of the shell.

This is valid if the shell is made of a linear elastic, isotropic, and homogeneous material.

To obtain the other form of the strain energy the product of the stresses and strains in (2.17) are also integrated through the thickness of the shell. But here they are integrated as they are. The integration of the stresses, through the thickness of the shell, results in the statically equivalent forces and moments which also forms the equilibrium equations, while the strains may be replaced by the deformations of the middle surface. By taking the first variation with respect to the displacements of the middle surface in both expressions of the strain energy and then comparing terms the following relations can be identified:

$$T_1 = \frac{Eh}{1-v^2}\left(\varepsilon_1 + v\varepsilon_2\right), \qquad\qquad T_2 = \frac{Eh}{1-v^2}\left(\varepsilon_2 + v\varepsilon_1\right)$$

$$M_1 = \frac{Eh^3}{12\left(1-v^2\right)}\left(\kappa_1 + v\kappa_2\right), \qquad M_2 = \frac{Eh^3}{12\left(1-v^2\right)}\left(\kappa_2 + v\kappa_1\right)$$

$$T_{12} = \frac{Eh}{2\left(1+v\right)}\left(\gamma + \frac{h^2}{6R_2}\tau\right), \qquad T_{21} = \frac{Eh}{2\left(1+v\right)}\left(\gamma\frac{h^2}{6R_1}\tau\right)$$

$$M_{12} = M_{21} = \frac{Eh^3}{12\left(1+v\right)}\tau$$

$$(2.19)$$

By substituting the relations between deformations and displacements of the middle surface, i.e. equations (2.13), into these relations and then these into the equilibrium equations presented in previous section the equilibrium between displacements is obtained. As a final remark the equilibrium equations expressed in displacements can also be obtained by equating to zero the first variation with respect to the displacements of the volume integral of the difference between the total potential energy and the kinetic energy. As long as free vibrations are considered the total potential energy is purely expressed by the strain energy in (2.18) while the kinetic energy is due to the oscillating mass of the shell. This method is known as Hamilton's principle.

Chapter

3

A Thin Walled Cylinder

In this chapter the shell theory will be specialised to a thin walled infinite cylinder making it possible to investigate the properties of free vibration of such geometry. On one hand this serves as an example of how the theory presented in previous section can be applied, and on the other hand the results serves as a limiting case of the thin walled torus which will be studied in next chapter. The results obtained in this chapter will be compared to results from classical Bernoulli-Euler beam theory describing some of the simplest free vibrational modes of a cylinder.
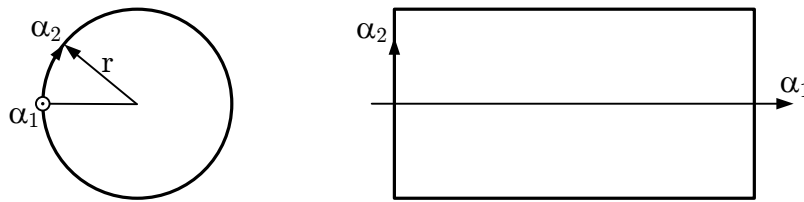
Figure 3.1: *The middle surface of the cylinder shell is wrapped by the curvilinear coordinate system, α_1 and α_2.*

The modelling of the cylinder shell follows the theory presented in previous chapter. From these relations a system of three coupled differential equations, formulated in the displacements of the shell, is obtained. The general solution to this system of equations is expected to be expressible as a product of three separate complex exponential functions. The three exponential functions are, respectively, function of the axial coordinate of the cylinder, the circumferential coordinate of the cylinder, and of the time. The cylinder is illustrated in figure 3.1 where the axial and circumferential coordinates are given in the curvilinear coordinates α_1 and α_2. Because the cylinder is a semi-closed shell the circumferential waves must be standing waves, having a wave length which multiplied with an integer gives the circumference of the cylinder. Without loss of generality such standing wave can be represented by an infinite sum of complex exponential functions, c.f. Fourier series. The axial waves are on the other hand either evanescent or travelling as long as the length of the cylinder is not bounded. Together this gives a solution on the form:

$$\mathbf{u}(\alpha_1, \alpha_2, t) = \begin{bmatrix} u \\ v \\ w \end{bmatrix} = \sum_{m=0}^{\infty} \mathrm{Re}\left\{\mathbf{a}_m e^{\frac{i m \alpha_2}{r}}\right\} \mathrm{Re}\left\{e^{\frac{k\alpha_1}{r}} e^{\frac{i\omega c_0 t}{r}}\right\} \tag{3.1}$$

where:　u, v, w　　　Axial, tangential, and normal displacements of the middle surface of the cylinder shell.

　　　　　k　　　　　Non-dimensional complex wave number.

　　　　　m　　　　　Circumferential mode number.

　　　　　$\mathbf{a}_m$　　　　Vector of complex amplitudes of vibrations.

　　　　　ω　　　　　Non-dimensional frequency.

　　　　　c_0　　　　　Speed of sound.

Note that α_1 and α_2 are scaled by r to ensure that k and m are non-dimensional. Similar t is scaled by $\frac{c_0}{r}$ to make ω non-dimensional. Later this scaling will show itself convenient. By substituting this solution into the system of differential equations a system of algebraic equations is formed. To investigate the dynamical properties of the cylinder shell, at one fundamental circumferential wave mode at the time, i.e. for one specific value of m, this system of equations can be arranged as a matrix-vector equation of the form:

$$\underset{3 \times 3}{\mathbf{M}}\,(k, \omega, m)\,\mathbf{a}_m = \mathbf{0} \tag{3.2}$$

According to Cramer's rule a nontrivial solution of such system exists if the determinant to the coefficient matrix is zero. So by taking the determinant and equating it to zero the relation between the wave number, k, and the frequency, ω, at the specified value of m, can be examined. By determining the wave number at different frequencies the so-called *dispersion curves* can be plotted. This dispersion diagram contains information about the transition between evanescent and travelling waves in the axial direction of the cylinder and how each wave evolves at different frequencies. The dispersion curves will be unique to the cylinder shell and to the specified circumferential mode number. To obtain this the relations presented in previous chapter will now be specialised to the geometry of a cylinder.

3.1　Geometrical Properties of a Thin Walled Cylinder

The geometry of the middle surface of a cylinder can be parameterised as:

$$\mathbf{r}(\alpha_1, \alpha_2) = \begin{bmatrix} r\cos\left(\frac{\alpha_2}{r}\right) \\ r\sin\left(\frac{\alpha_2}{r}\right) \\ \alpha_1 \end{bmatrix} \tag{3.3}$$

Applying this to equations (2.6) the Lamé parameters of the cylinder are:

$$A_1(\alpha_1, \alpha_2) = \sqrt{\left(\frac{\partial x}{\partial \alpha_1}\right)^2 + \left(\frac{\partial y}{\partial \alpha_1}\right)^2 + \left(\frac{\partial z}{\partial \alpha_1}\right)^2} = \sqrt{1^2} = 1$$

$$A_2(\alpha_1, \alpha_2) = \sqrt{\left(\frac{\partial x}{\partial \alpha_2}\right)^2 + \left(\frac{\partial y}{\partial \alpha_2}\right)^2 + \left(\frac{\partial z}{\partial \alpha_2}\right)^2} = \sqrt{\left(-\sin\left(\frac{\alpha_2}{r}\right)\right)^2 + \left(\cos\left(\frac{\alpha_2}{r}\right)\right)^2} = \sqrt{1^2} = 1 \tag{3.4}$$

The radii of curvature can easily be guessed to:

$$R_1 = \infty \tag{3.5}$$

$$R_2 = r \tag{3.6}$$

$$R_1 = \infty$$

$$R_2 = r \tag{3.7}$$

But this can also be verified by equations (2.7) through (2.10).

3.2 Deformations of the Middle Surface of the Cylinder

The deformations of the middle surface of the cylinder are determined by substituting the Lamé parameters and the radii of curvature from above into the relations in (2.13):

$$\varepsilon_1 = \frac{\partial u}{\partial \alpha_1}$$

$$\varepsilon_2 = \frac{\partial v}{\partial \alpha_2} + \frac{1}{r} w$$

$$\gamma = \frac{\partial u}{\partial \alpha_2} + \frac{\partial v}{\partial \alpha_1}$$

$$\kappa_1 = -\frac{\partial^2 w}{\partial \alpha_1^2} \tag{3.8}$$

$$\kappa_2 = \frac{1}{r} \frac{\partial v}{\partial \alpha_2} - \frac{\partial^2 w}{\partial \alpha_2^2}$$

$$\tau = \frac{1}{r} \frac{\partial v}{\partial \alpha_1} - \frac{\partial^2 w}{\partial \alpha_1 \partial \alpha_2}$$

3.3 Equilibrium Equations of an Element of the Cylinder Shell

Similar to the deformations, the force equilibrium equations of the cylinder shell are determined by substituting the Lamé parameters and the radii of curvature into equations (2.15):

$$0 = \frac{\partial T_1}{\partial \alpha_1} + \frac{\partial T_{21}}{\partial \alpha_2} + q_1$$

$$0 = \frac{\partial T_{12}}{\partial \alpha_1} + \frac{\partial T_2}{\partial \alpha_2} + \frac{N_2}{r} + q_2 \tag{3.9}$$

$$0 = \frac{\partial N_1}{\partial \alpha_1} + \frac{\partial N_2}{\partial \alpha_2} - \frac{T_2}{r} + q_n$$

The forces N_1 and N_2 are determined from the first two of the moment equilibrium equations in (2.16):

$$N_1 = \frac{\partial M_1}{\partial \alpha_1} + \frac{\partial M_{21}}{\partial \alpha_2}$$

$$N_2 = \frac{\partial M_{12}}{\partial \alpha_1} + \frac{\partial M_2}{\partial \alpha_2}$$

(3.10)

And they are substituted into the force equilibrium equations above:

$$0 = \frac{\partial T_1}{\partial \alpha_1} + \frac{\partial T_{21}}{\partial \alpha_2} + q_1$$

$$0 = \frac{\partial T_{12}}{\partial \alpha_1} + \frac{\partial T_2}{\partial \alpha_2} + \frac{1}{r}\left(\frac{\partial M_{12}}{\partial \alpha_1} + \frac{\partial M_2}{\partial \alpha_2}\right) + q_2$$

$$0 = \frac{\partial^2 M_1}{\partial \alpha_1^2} + \frac{\partial^2 M_{21}}{\partial \alpha_1 \alpha_2} + \frac{\partial^2 M_{12}}{\partial \alpha_1 \alpha_2} + \frac{\partial^2 M_2}{\partial \alpha_2^2} - \frac{T_2}{r} + q_n$$

(3.11)

The forces and moments are then eliminated by substituting from the relations in (2.19):

$$0 = \frac{\partial \varepsilon_1}{\partial \alpha_1} + v\frac{\partial \varepsilon_2}{\partial \alpha_1} + \frac{1-v}{2}\frac{\partial \gamma}{\partial \alpha_2} + \frac{1-v^2}{Eh}q_1$$

$$0 = \frac{1-v}{2}\left(\frac{\partial \gamma}{\partial \alpha_1} + \frac{h^2}{6r}\frac{\partial \tau}{\partial \alpha_1}\right) + \frac{\partial \varepsilon_2}{\partial \alpha_2} + v\frac{\partial \varepsilon_1}{\partial \alpha_2} +$$

$$+ \frac{(1-v)\,h^2}{12r}\frac{\partial \tau}{\partial \alpha_1} + \frac{h^2}{12r}\left(\frac{\partial \kappa_2}{\partial \alpha_2} + v\frac{\partial \kappa_1}{\partial \alpha_2}\right) + \frac{1-v^2}{Eh}q_2$$

(3.12)

$$0 = \frac{h^2}{12}\left(\frac{\partial^2 \kappa_1}{\partial \alpha_1^2} + v\frac{\partial^2 \kappa_2}{\partial \alpha_1^2}\right) + \frac{(1-v)\,h^2}{6}\frac{\partial^2 \tau}{\partial \alpha_1 \partial \alpha_2} +$$

$$+ \frac{h^2}{12}\left(\frac{\partial^2 \kappa_2}{\partial \alpha_2^2} + v\frac{\partial^2 \kappa_1}{\partial \alpha_2^2}\right) - \frac{\varepsilon_2 + v\varepsilon_1}{r} + \frac{1-v^2}{Eh}q_n$$

To obtain the equilibrium equations expressed in displacements, the deformations of the middle surface are substituted by the relations in (3.8):

$$0 = \frac{\partial^2 u}{\partial \alpha_1^2} + v\left(\frac{\partial^2 v}{\partial \alpha_1 \partial \alpha_2} + \frac{1}{r}\frac{\partial w}{\partial \alpha_1}\right) + \frac{1-v}{2}\left(\frac{\partial^2 u}{\partial \alpha_2^2} + \frac{\partial^2 v}{\partial \alpha_1 \partial \alpha_2}\right) + \frac{1-v^2}{Eh}q_1$$

$$0 = \frac{1-v}{2}\left(\frac{\partial^2 u}{\partial \alpha_1 \partial \alpha_2} + \frac{\partial^2 v}{\partial \alpha_1^2} + \frac{h^2}{6r}\left(\frac{1}{r}\frac{\partial^2 v}{\partial \alpha_1^2} - \frac{\partial^3 w}{\partial \alpha_1^2 \partial \alpha_2}\right)\right) + \frac{\partial^2 v}{\partial \alpha_2^2} + \frac{1}{r}\frac{\partial w}{\partial \alpha_2} + v\frac{\partial^2 u}{\partial \alpha_1 \partial \alpha_2} +$$

$$+\frac{(1-v)\,h^2}{12r}\left(\frac{1}{r}\frac{\partial^2 v}{\partial \alpha_1^2} - \frac{\partial^3 w}{\partial \alpha_1^2 \partial \alpha_2}\right) + \frac{h^2}{12r}\left(\left(\frac{1}{r}\frac{\partial^2 v}{\partial \alpha_2^2} - \frac{\partial^3 w}{\partial \alpha_2^3}\right) - v\frac{\partial^3 w}{\partial \alpha_1^2 \partial \alpha_2}\right) + \frac{1-v^2}{Eh}q_2 \qquad (3.13)$$

$$0 = \frac{h^2}{12}\left(-\frac{\partial^4 w}{\partial \alpha_1^4} + v\left(\frac{1}{r}\frac{\partial^3 v}{\partial \alpha_1^2 \partial \alpha_2} - \frac{\partial^4 w}{\partial \alpha_1^2 \partial \alpha_2^2}\right)\right) + \frac{(1-v)\,h^2}{6}\left(\frac{1}{r}\frac{\partial^3 v}{\partial \alpha_1^2 \partial \alpha_2} - \frac{\partial^4 w}{\partial \alpha_1^2 \partial \alpha_2^2}\right) +$$

$$+\frac{h^2}{12}\left(\frac{1}{r}\frac{\partial^3 v}{\partial \alpha_2^3} - \frac{\partial^4 w}{\partial \alpha_2^4} - v\frac{\partial^4 w}{\partial \alpha_1^2 \partial \alpha_2^2}\right) - \frac{1}{r}\frac{\partial v}{\partial \alpha_2} - \frac{1}{r^2}w - \frac{v}{r}\frac{\partial u}{\partial \alpha_1} + \frac{1-v^2}{Eh}q_n$$

As a final step before the general solution is substituted into the equilibrium equations the intensity of the forcing of the middle surface, **q**, must be considered. The scope of this chapter is, as mentioned, to investigate the free vibration properties of a cylinder shell. Because the equilibrium equations from above are valid for the middle surface of an infinitesimal element of the shell and because no other body forces or surface tractions are considered than the inertia force due to the free vibration the intensity of **q** is:

$$\mathbf{q} = \frac{\partial\left(h\rho\dot{\mathbf{u}}\right)}{\partial t} = h\rho\frac{\partial^2 \mathbf{u}}{\partial t^2} = h\rho\frac{\partial^2}{\partial t^2}\begin{bmatrix} u \\ v \\ w \end{bmatrix} \qquad (3.14)$$

where: ρ density.

By substituting this into the equilibrium equations derived above the following can be obtained:

$$\begin{bmatrix} \begin{array}{c} \frac{\partial^2}{\partial \alpha_1^2} + \frac{1-v}{2}\frac{\partial^2}{\partial \alpha_2^2} + \\ + \frac{(1-v^2)\rho}{E}\frac{\partial^2}{\partial t^2} \end{array} & \frac{1+v}{2}\frac{\partial^2}{\partial \alpha_1 \partial \alpha_2} & \frac{v}{r}\frac{\partial}{\partial \alpha_1} \\[3ex] \frac{1+v}{2}\frac{\partial^2}{\partial \alpha_1 \partial \alpha_2} & \begin{array}{c} \frac{1-v}{2}\left(1+\frac{h^2}{3r^2}\right)\frac{\partial^2}{\partial \alpha_1^2} + \\ + \left(1+\frac{h^2}{12r^2}\right)\frac{\partial^2}{\partial \alpha_2^2} + \frac{(1-v^2)\rho}{E}\frac{\partial^2}{\partial t^2} \end{array} & \begin{array}{c} -\frac{h^2}{12r}\frac{\partial^3}{\partial \alpha_2^3} - \\ -\frac{(2-v)h^2}{12r}\frac{\partial^3}{\partial \alpha_1^2 \partial \alpha_2} + \frac{1}{r}\frac{\partial}{\partial \alpha_2} \end{array} \\[4ex] -\frac{v}{r}\frac{\partial}{\partial \alpha_1} & \begin{array}{c} \frac{h^2}{12r}\frac{\partial^3}{\partial \alpha_2^3} + \\ + \frac{(2-v)h^2}{12r}\frac{\partial^3}{\partial \alpha_1^2 \partial \alpha_2} - \frac{1}{r}\frac{\partial}{\partial \alpha_2} \end{array} & \begin{array}{c} -\frac{h^2}{12}\frac{\partial^4}{\partial \alpha_1^4} - \frac{h^2}{12}\frac{\partial^4}{\partial \alpha_2^4} - \frac{1}{r^2} - \\ -\frac{h^2}{6}\frac{\partial^4}{\partial \alpha_1^2 \partial \alpha_2^2} + \frac{(1-v^2)\rho}{E}\frac{\partial^2}{\partial t^2} \end{array} \end{bmatrix}\begin{bmatrix} u \\ v \\ w \end{bmatrix} = \mathbf{0} \qquad (3.15)$$

Here the matrix can be regarded as a differential operator acting on the displacements of the cylinder shell. Next step is to substitute the solution.

3.4 Solving the Equations of Equilibrium of the Cylinder Shell

If a single term of the general solution in (3.1), i.e. for at specific circumferential mode number, m, is substituted into the system of partial differential equations in (3.15) they become algebraic. Then, if these algebraic equations are also divided with the exponential functions of this single term of the general solution, the following can be obtained:

$$\mathbf{M}\mathbf{a}_m = \mathbf{0}$$

$$\Updownarrow$$

$$
\begin{bmatrix}
\frac{k^2}{r^2} - \frac{1-\nu}{2}\frac{m^2}{r^2} - \frac{(1-\nu^2)\rho\omega^2 c_0^2}{Er^2} & \frac{1+\nu}{2}\frac{imk}{r^2} & \frac{\nu k}{r^2} \\[2ex]
\frac{1+\nu}{2}\frac{imk}{r^2} & \frac{1-\nu}{2}\left(1+\frac{h^2}{3r^2}\right)\frac{k^2}{r^2} - \left(1+\frac{h^2}{12r^2}\right)\frac{m^2}{r^2} - \frac{(1-\nu^2)\rho\omega^2 c_0^2}{Er^2} & \frac{h^2}{12r}\frac{im^3}{r^3} - \frac{(2-\nu)h^2}{12r}\frac{imk^2}{r^3} + \frac{im}{r^2} \\[2ex]
-\frac{\nu k}{r^2} & -\frac{h^2}{12r}\frac{im^3}{r^3} + \frac{(2-\nu)h^2}{12r}\frac{imk^2}{r^3} - \frac{im}{r^2} & -\frac{h^2}{12}\frac{k^4}{r^4} - \frac{h^2}{12}\frac{m^4}{r^4} - \frac{1}{r^2} + \frac{h^2}{6}\frac{m^2 k^2}{r^4} - \frac{(1-\nu^2)\rho\omega^2 c_0^2}{Er^2}
\end{bmatrix}
\begin{bmatrix} a_m \\ b_m \\ c_m \end{bmatrix} = \mathbf{0} \quad (3.16)
$$

As mentioned in the beginning of this chapter, solutions where $\mathbf{a}_m \neq \mathbf{0}$ exists only if the determinant of $\mathbf{M}$ is zero. Before expanding the determinant it will though show itself convenient to multiply all terms in the matrix with the common factor r^2 and to multiply the second row with i and then also divide second column with i. The combination of the last two manipulations remains the determinant unchanged while the first do not change the relation between each of the rows or columns of the matrix. Along with this the transformation $\frac{h}{r} = \delta$ is introduced and it is recognised that $c_0 = \sqrt{\frac{E}{\rho}}$. After also introducing these manipulations the following equation must be solved:

$$|\mathbf{M}| = 0$$

$$\Updownarrow$$

$$
\begin{vmatrix}
k^2 - \frac{1-\nu}{2}m^2 - (1-\nu^2)\omega^2 & \frac{1+\nu}{2}mk & \nu k \\[2ex]
-\frac{1+\nu}{2}mk & \frac{1-\nu}{2}\left(1+\frac{\delta^2}{3}\right)k^2 - \left(1+\frac{\delta^2}{12}\right)m^2 - (1-\nu^2)\omega^2 & -\frac{\delta^2}{12}m^3 + \frac{(2-\nu)}{12}\delta^2 mk^2 - m \\[2ex]
-\nu k & -\frac{\delta^2}{12}m^3 + \frac{(2-\nu)}{12}\delta^2 mk^2 - m & -\frac{\delta^2}{12}k^4 - \frac{\delta^2}{12}m^4 - 1 + \frac{\delta^2}{6}m^2 k^2 - (1-\nu^2)\omega^2
\end{vmatrix} = 0 \quad (3.17)
$$

The manipulations between (3.16) and (3.17) reveal that the only material dependency on the determinant is Poisson's ratio. It can also be seen that the only important geometrical property of the cylinder is the ratio, δ, between the shell thickness and the radius of the cylinder.

Expansion of the determinant results in a so-called *dispersion polynomial* of eighth order of k and sixth order of ω. This polynomial can be solved numerically making it possible to plot the dispersion curves for specified values of m. A plot of the dispersion curves obtained from this cylinder shell model, related to the first three circumferential mode numbers, is seen as the thin curves in figure 3.2. In this plot $\nu = 0.3$ which is common to most metals. The relation between the shell thickness and the radius of the cylinder is given in the headline of the figure.
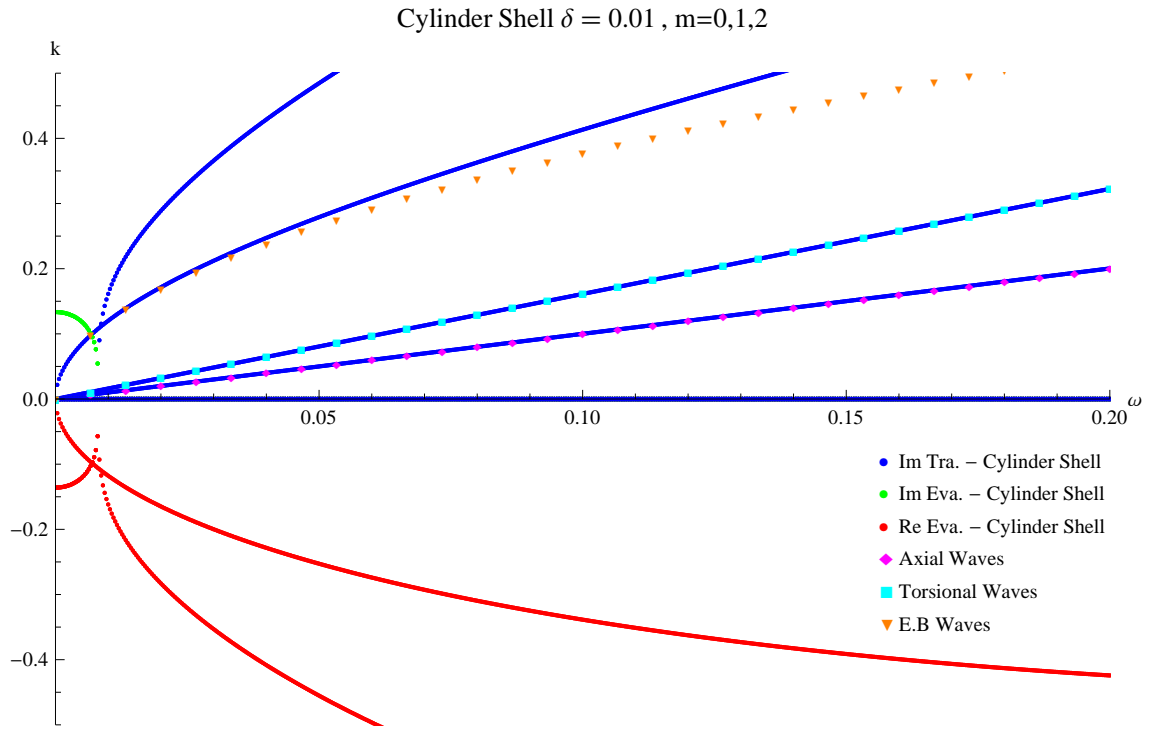
Figure 3.2: *The figure shows dispersions curves from the first three circumferential mode numbers.*

3.5 Correlation Between the Cylinder Shell and Classical Beam Theory

The two straight curves in figure 3.2 are related to $m = 0$, the curved one, cutting on at $\omega = 0$, is related to $m = 1$, while the one cutting on just below $\omega = 0.01$ relates to $m = 2$. To get a physical understanding of the vibrational displacement pattern of the cylinder shell, present at these circumferential modes, a closer study of the solution, substituted into the equilibrium equations, can be helpful. Naturally the most interesting part of the solution, in this context, is the exponential function regarding the circumferential mode number along with its vector of vibrational amplitudes. When $m = 0$ this exponential function gives:

$$\mathbf{a}_0 e^{\frac{i 0 \alpha_2}{r}} = \mathbf{a}_0 = \begin{bmatrix} a_0 \\ b_0 \\ c_0 \end{bmatrix} \tag{3.18}$$

Thus the displacements along the circumference of the cylinder are uniform. And because the displacements are related to the curvilinear coordinate system in figure 3.1 this uniform circumferential displacement pattern can be illustrated as in figure 3.3.
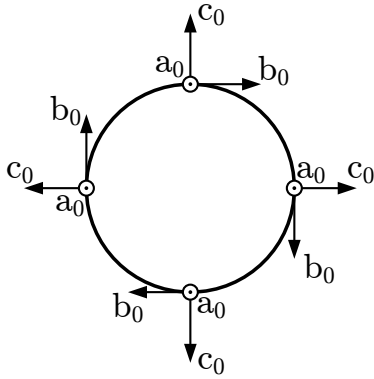
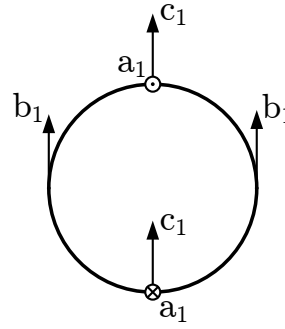**Figure 3.3:** *The displacements along the circumference at m = 0 are uniform.*

Figure 3.4: *The displacements along the circumference at m = 1 have a period of 2π.*

From the matrix in (3.16) it can also be seen that if $m = 0$ then b_0 is uncoupled from a_0 and c_0 while a_0 and c_0 are coupled due to Poisson's ratio. Thus one solution can be of the form $\mathbf{a}_0 = \begin{bmatrix} 0 & b_0 & 0 \end{bmatrix}^T$ and another can be $\mathbf{a}_0 = \begin{bmatrix} a_0 & 0 & b_0 \end{bmatrix}^T$. The first one corresponds to torsional vibration of the cylinder. This vibrational mode can also be modelled through classical beam theory. When modelled so the following partial differential equation can be obtained (cf. Rao [2003]):

$$GJ\frac{\partial^2\theta\,(x,t)}{\partial x^2} = I_0\frac{\partial^2\theta\,(x,t)}{\partial t^2} \tag{3.19}$$

where:
G Shear modulus.

J Polar moment of inertia.

θ Angle of twist of the beam.

x Coordinate along the axis of rotation of the beam.

I_0 Polar mass moment of inertia.

The polar mass moment of inertia can be written as $I_0 = \rho J$, the coordinate along the axis of rotation of the beam can be written as $x = \alpha_1$, and the angle of twist can in relation to the shell model of the cylinder be written as $\theta = \frac{v}{r}$. If the general solution in (3.1) is substituted into the differential equation and the equation then also is divided with this solution the following is obtained:

$$G\frac{\partial^2 v}{\partial\alpha_1^2} = \rho\frac{\partial^2 v}{\partial t^2} \tag{3.20}$$

$$\Downarrow$$

$$\frac{E}{2\,(1+v)}\frac{k^2}{r^2} = -\frac{\rho\omega^2 c_0^2}{r^2} = -\frac{\omega^2 E}{r^2} \tag{3.21}$$

$$\Downarrow$$

$$k = \pm\sqrt{2\,(1+v)}\,i\omega \tag{3.22}$$

The positive imaginary part of this wave number is plotted as function of the frequency as the cyan square marks in figure 3.2 and shows a close correlation to one of the branches of the dispersion curves of the cylinder shell model.

The other solution, $\mathbf{a}_0 = [a_0 \quad 0 \quad b_0]^T$, corresponds to a wave mode of coupled axial and breathing vibrations. As mentioned earlier the coupling is due to Poisson's ratio. Physically it means that if the cylinder is either stretched or compressed in its axial direction, the cross section will either contract or expand in the radial direction. Such vibrational mode can also, implicitly, be modelled through classical beam theory. If a beam is subjected to axial vibration the governing partial differential equation is (cf. Rao [2003]):

$$EA\frac{\partial^2 u(x,t)}{\partial x^2} = \rho A\frac{\partial^2 u(x,t)}{\partial t^2} \tag{3.23}$$

where: A Cross sectional area.

   u Axial displacement.

When modelled so nothing has been assumed about the area changes of the cross section. Thus the boundary of the cross section of the beam is free of tractions which implicitly mean that it is free to expand or contract as needed. This is exactly the same situation as when the cylinder shell is excited in a axial vibration mode which is coupled to breathing vibrations. Applying same manipulations to the above differential equation as to the differential equation governing the torsional vibration the following is gained:

$$E\frac{\partial^2 u}{\alpha_1^2} = \rho\frac{\partial^2 u}{\partial t^2} \tag{3.24}$$

$$\Downarrow$$

$$E\frac{k^2}{r^2} = -\frac{\rho\omega^2 c_0^2}{r^2} = -\frac{\omega^2 E}{r^2} \tag{3.25}$$

$$\Downarrow$$

$$k = \pm i\omega \tag{3.26}$$

Again the positive imaginary part of the wave number is plotted against the frequency as the purple square marks in figure 3.2. Also here a close correlation is seen the one of the branches of the dispersion curves of the shell model.

Now one possible vibration mode when $m = 1$ will be studied. The interesting term of the general solution in (3.1) is in this case:

$$\mathbf{a}_1 e^{\frac{i1\alpha_2}{r}} = \begin{bmatrix} a_1 \\ b_1 \\ c_1 \end{bmatrix}\left(\cos\left(\tfrac{\alpha_2}{r}\right) + i\sin\left(\tfrac{\alpha_2}{r}\right)\right) \tag{3.27}$$

This solution is obviously periodic in the circumference of the cylinder and has a period of 2π. Indeed it is possible that $\mathbf{a}_1$ can be of the form:

$$\mathbf{a}_1 = \mathrm{Re}\{\mathbf{a}_1\} + i\mathrm{Im}\{\mathbf{a}_1\} = \begin{bmatrix} 0 \\ b_1 \\ 0 \end{bmatrix} + i\begin{bmatrix} a_1 \\ 0 \\ c_1 \end{bmatrix} \tag{3.28}$$

If so, then the tangential displacement has a phase shift of π to the normal and axial displacement of the surface of the cylinder shell. Such pattern is illustrated in figure 3.4. A displacement field well known from the classical beam theory, which is almost encompassed by this displacement pattern, is the bending of a beam subjected to the kinematic constraints due to Kirchhoff. As mentioned previously in this thesis, the cross section of a bending Bernoulli-Euler beam is kinematically constraint to remain plane and perpendicular to the centre line of the beam. This is almost the same as assuming that the cross section moves as a rigid body and rotates just as much as the centre line of the beam. Why it is just almost and not exactly the same will be discussed later in this section. But for the time being the deviation between these two formulations will be neglected. Thus it is reasonable to assume that some appropriate values and signs of a_1, b_1, and c_1 exist, such that the motion of the cross section in figure 3.4 will resemblance the motion of the cross section in a Bernoulli-Euler beam subjected to bending vibrations. The governing partial differential equation of a beam subjected to free bending vibrations can be written as (cf. Rao [2003]):

$$EI\frac{\partial^4 w(x,t)}{\partial x^4} = -\rho A\frac{\partial^2 w(x,t)}{\partial t^2} \tag{3.29}$$

where: I Moment of inertia.

           w Displacement of the beam normal to its centre line.

If the same substitutions and manipulations are made to this equation as to the previous torsional and axial vibration cases and it is noted that for a thin walled cylinder $A = 2\pi r h$ and $I = \pi r^3 h$ the following is obtained:

$$EI\frac{\partial^4 w}{\partial \alpha_1^4} = -\rho A\frac{\partial^2 w}{\partial t^2} \tag{3.30}$$

$$\Downarrow$$

$$E\pi r^3 h\frac{k^4}{r^4} = \rho 2\pi r h\frac{\omega^2 c_0^2}{r^2} = 2\pi h\frac{\omega^2 E}{r} \tag{3.31}$$

$$\Downarrow$$

$$k = \pm 2^{\frac{1}{4}}\sqrt{\omega}i \quad \bigvee \quad k = \pm 2^{\frac{1}{4}}\sqrt{\omega} \tag{3.32}$$

The positive imaginary part of this solution has also been plotted and is seen as the orange triangle markers in figure 3.2. Especially in the low-frequency range a fair correlation is again seen between the beam theory and the results obtained through the shell theory.

Now returning to the two formulations of the kinematic constraints enforced on the bending beam. The difference of these two assumptions is that the kinematic assumption due to Kirchhoff only assumes that the cross section remains plane. Thus, on the compression side of the centre line of the bending beam the cross section will tend to expand while on the elongating side of the centre line the cross section will contract. The result of this is that even though the cross section is constraint to remain plane it is free to change shape as long as the boundaries of the cross section are free of tractions. Thus, the cross section in a Bernoulli-Euler beam does not move as a rigid body. It is though possible to demonstrate the impact if actually assuming that the cross section moves as a rigid body and rotates just as much as the centre line. This can be done by requiring:

$$\mathbf{a}_1 = \text{Re}\{\mathbf{a}_1\} + i\,\text{Im}\{\mathbf{a}_1\} = \begin{bmatrix} 0 \\ W \\ 0 \end{bmatrix} + i \begin{bmatrix} -r\frac{\partial W}{\partial \alpha_1} \\ 0 \\ W \end{bmatrix} \tag{3.33}$$

where: W Amplitude of displacement of the bending vibration mode.

Here it is also assumed that the amplitude of displacements are sufficiently small, making it possible to substitute the angle of rotation by the slope of the centre line. This is also assumed in the classical beam theory. Then, under these kinematic constraints, the deformations of the middle surface of the cylinder can be determined from (3.8) and afterwards substituted into equation (2.18) to determine the strain energy accumulated under the deformation of the shell. This strain energy can then be equated to the kinetic energy of the vibrating shell and through Hamilton's principle, which has also been mentioned previously, the following differential equation can be derived (the explicit mathematical manipulations following to this equation is though omitted here):

$$\frac{EI}{1-v^2}\left(1+\frac{h^2}{12r^2}\right)\frac{\partial^4 W}{\partial \alpha_1^4} = \rho I \frac{\partial^4 W}{\partial \alpha_1^2 \partial t^2} - \rho A \frac{\partial^2 W}{\partial t^2} \tag{3.34}$$

Except of the denominator on left-hand side of this differential equation this was also derived by Lord Reyleigh in his book *The Theory of Sound*, Rayleigh [1894]. Again, if the differential equation is exposed to same manipulations as previous the following can be obtained:

$$\frac{EI}{1-v^2}\left(1+\frac{h^2}{12r^2}\right)\frac{k^4}{r^4} = -\rho I \frac{k^2 \omega^2 c_0^2}{r^4} + \rho A \frac{\omega^2 c_0^2}{r^2} \tag{3.35}$$

$$\Downarrow$$

$$\frac{1}{1-v^2}\left(1+\frac{\delta^2}{12}\right)k^4 = -k^2\omega^2 + 2\omega^2 = \left(2-k^2\right)\omega^2 \tag{3.36}$$

This equation can be further simplified by considering the smallness of δ^2 compared to 1 and the smallness of k^2 compared to 2, cf. figure 3.2. Thus the wave number is:

$$\frac{1}{1-v^2}k^4 = 2\omega^2 \tag{3.37}$$

$$\Downarrow$$

$$k = \pm\left(2\left(1-v^2\right)\right)^{\frac{1}{4}}\sqrt{\omega}\,i \quad \bigvee \quad k = \pm\left(2\left(1-v^2\right)\right)^{\frac{1}{4}}\sqrt{\omega} \tag{3.38}$$

Compared to the wave numbers determined from the Bernoulli-Euler beam theory, cf. equation (3.32), these results are corrected due to the Poisson coupling. But if $v = 0.3$ then the deviation on the wave numbers is less than 3 % and thus is lower than the possible error on the shell theory itself, cf. section 2.1 on page 5.

   With these final remarks the derived shell model of a thin walled cylinder is regarded as valid in comparison to classical beam theory. The dispersion curves in figure 3.2 will thus be used for validation of the modelling of the thin walled toroidal shell which will be presented in next chapter.

Chapter

4

A Thin Walled Torus

In this chapter the free vibration properties of a thin walled infinite torus will be investigated. The torus will be modelled as a thin shell and the modelling will follow the same sequence of event as in previous chapter where the thin walled cylinder where studied. Though, due to the slightly more complex geometry, the derived equations will be significantly more cumbersome and thus they cannot be presented in same explicit extend as when deriving the equations of the cylinder. For same reason the derivations are facilitated by the mathematical software tool Mathematica® *making it possible to get through with the analytic derivation of the results. Finally the results will be compared to results obtained through curved beam theory and to the results of the cylinder analysis which acts as the limiting case of the torus.*
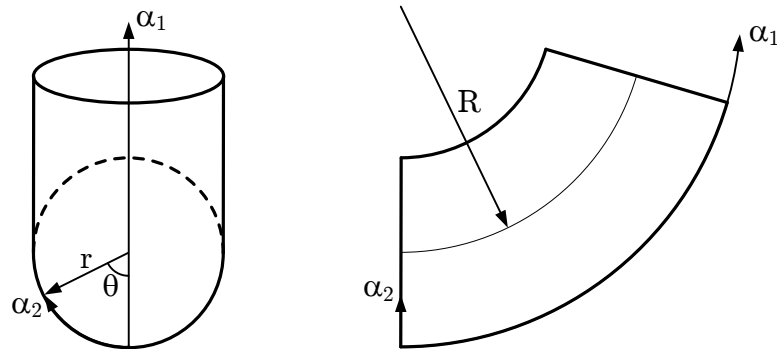

Figure 4.1: *The middle surface of the toroidal shell is wrapped by the curvilinear coordinate system,* α_1 *and* α_2*.*

The toroidal shell is, like the cylinder shell, a semi-infinite shell. Thus the toroidal shell is closed in its circumferential direction while it is unbounded in its axial direction. Consequently the general solution to the problem of determining the free vibration displacements is expected to be identical to the corresponding general solution to the cylinder shell. The solution is found as equation (3.1) on page 15. But here the curvilinear coordinates are wrapping the middle surface of the toroidal shell as illustrated in figure 4.1. When studying the cylinder shell the dispersion curves where determined for one value of the circumferential mode number at the time. This made it possible to study some of the simplest vibrational modes of the cylinder and compare them to results obtained through classical beam theory. This is possible because the vibrational modes associated to the different circumferential vibration modes do not interact. In the cylinder case the bending mode do not interact with e.g. the torsional mode nor the

axial mode. But if the cylinder then is bent, forming a torus, these vibrational modes start to interact. If the toroidal shell is e.g. excited in its axial direction the vibrations will unavoidable excite bending vibrations. In this case the displacements of the neutral axis associated with the bending will be parallel to the plane in which the torus is lying and thus this bending mode will be recognised as in-plane bending. On the other hand if the toroidal shell is excited in a torsional mode these vibrations will immediately excite bending which displace the neutral axis out of the plane of the torus. Consequently this bending mode will be recognised as out-off-plane bending.

These considerations indicate that even the simplest vibrational modes of the toroidal shell cannot be attained by a single circumferential mode number but are a result of coupling between several, or at least two, circumferential mode numbers. Based on the experiences from the analysis of the cylindrical shell it is then imaginable that the above discussed interaction between the axial vibration mode and the in-plane bending mode or the torsional vibration mode and the out-off-plane bending mode are both due to coupling between $m = 0$ and $m = 1$. Thus, under the coupling between in-plane bending and axial vibration, the kinematic constraints on a cross section of the torus is that the bending contribution makes it move as a rigid body, oscillating in direction of the centre of the torus, and rotate like the centre line. At same time the axial vibration contribution makes the cross section oscillate in the axial direction of the torus while it is free to expand and contract due to Poisson's coupling. Similar, under the coupling between out-off-plane bending and torsion vibration, the bending contribution makes the cross section move as a rigid body, oscillating normal to the plane of the torus, and rotates like the centre line. Along with this the torsion contribution makes the cross section twist around the centre line. In equation (3.28) on page 23 a possible structure of the amplitude vector, $\mathbf{a}_m$, at $m = 1$ is presented. If this is substituted into (3.27) and then, in accordance to the general solution in (3.1), the real part is extracted the following is obtained:

$$\text{Re}\left\{\left(\begin{bmatrix} 0 \\ b_1 \\ 0 \end{bmatrix} + i \begin{bmatrix} a_1 \\ 0 \\ c_1 \end{bmatrix}\right)\left(\cos\left(\tfrac{\alpha_2}{r}\right) + i\sin\left(\tfrac{\alpha_2}{r}\right)\right)\right\} = \begin{bmatrix} u_1 \\ v_1 \\ w_1 \end{bmatrix}\begin{bmatrix} \sin(\theta) \\ \cos(\theta) \\ \sin(\theta) \end{bmatrix} \tag{4.1}$$

where: $\qquad u_1 = -a_1, \quad v_1 = b_1, \quad w_1 = -c_1.$

$\qquad\qquad\quad \theta = \tfrac{\alpha_2}{r}.$

Referring to the origin of the curvilinear coordinates in figure 4.1 this corresponds to out-off-plane bending. Along with the solution related to $m = 0$ the solution of coupled out-off-plane bending and torsional vibrations can then be expected to be of the form:

$$\mathbf{u}_{oop}(\alpha_1, \theta, t) = \left(\mathbf{u}_0 + \mathbf{u}_1 \begin{bmatrix} \sin(\theta) \\ \cos(\theta) \\ \sin(\theta) \end{bmatrix}\right)\text{Re}\left\{e^{\tfrac{k\alpha_1}{r}} e^{\tfrac{i\omega c_0 t}{r}}\right\} \tag{4.2}$$

It is though equally possible that $\mathbf{a}_1$ can be of the form:

$$\mathbf{a}_1 = \text{Re}\{\mathbf{a}_1\} + i\,\text{Im}\{\mathbf{a}_1\} = \begin{bmatrix} a_1 \\ 0 \\ c_1 \end{bmatrix} + i \begin{bmatrix} 0 \\ b_1 \\ 0 \end{bmatrix} \tag{4.3}$$

Substituted into the solution and relating to figure 4.1 it is seen that this corresponds to in-plane bending. The solution of coupled in-plane bending and axial vibration can then be expected to have the form:

$$\mathbf{u}_{ip}(\alpha_1, \theta, t) = \left(\mathbf{u}_0 + \mathbf{u}_1 \begin{bmatrix} \cos(\theta) \\ \sin(\theta) \\ \cos(\theta) \end{bmatrix} \right) \mathrm{Re} \left\{ e^{\frac{k\alpha_1}{r}} e^{\frac{i\omega c_0 t}{r}} \right\} \tag{4.4}$$

These two mode can also be regarded as, respectively, antisymmetric and symmetric modes with respect to a line between $\theta = 0$ and $\theta = \pi$. Thus the out-off-plane bending mode is antisymmetric while the in-plane bending mode is symmetric. In accordance to Akhilesh K. Jha [2002] it has been shown that generally symmetric and antisymmetric vibration mode, of a toroidal shell, can be studied independently, because they do not interact. Thus these two modes are regarded as the two fundamental vibrational modes of the torus and are expected to be comparable to corresponding results obtained through curved beam theory.

Similar to the development of the cylinder shell model it is also here necessary to establish the three partial differential equations of equilibrium expressed in displacements of the middle surface of the shell. When the solution, representing either in-plane bending or out-off-plane bending, is substituted into the equilibrium equations they become algebraic containing six unknowns due to $\mathbf{u}_0$ and $\mathbf{u}_1$. To solve this, additional equations must be introduces. This can be done by applying *Galerkin's method.* Galerkin's method is based on the principle that the virtual work performed by a virtual displacement away from a stationary configuration is zero[1]. If, at one hand, a trial solution of the following form is substituted into the equilibrium equations:

$$\widetilde{\mathbf{u}}_M = \sum_{m=0}^{M} \mathbf{u}_m \boldsymbol{\phi}_m \tag{4.5}$$

where: $\mathbf{u}_m$ Vector of constants.

   $\boldsymbol{\phi}_m$ Vector of base functions.

And, at the other hand, the virtual displacement of the displacement field can be represented by any of the vectors of base functions. Then, regardless of which one of the vectors of base functions is used to represent the virtual displacement, the resulting virtual work is required to remain zero, the following equations are obtained (cf. Irving H. Shames [1991]):

$$\int_V \mathbf{L}\widetilde{\mathbf{u}}_M \boldsymbol{\phi}_m \, dV = 0, \qquad m = 0, 1, 2, ..., M \tag{4.6}$$

where: $\mathbf{L}$ Differential operator.

   V Volume of the continuum under consideration.

The differential operator, $\mathbf{L}$, is in this case obtain by regarding the equations of equilibrium as a differential operator acting on the trial solution $\widetilde{\mathbf{u}}_M$. Because (4.6) holds three equations for each value of m and, in accordance to (4.5), each value of m deliverers three unknowns, $\mathbf{u}_m$, the number of equations and unknowns are equal.

With this outline of a strategy, making it possible to study the interaction between different circumferential mode numbers, the differential equations governing the displacements of the toroidal shell will be established. Thus, the first step is to determine the Lamé parameters and radii of curvature of the toroidal shell.

---

[1]Due to D'Alembert's principle, making it possible to regard the dynamical contribution to the equilibrium equations as inertia forces, this stationary principle still holds in this case.

4.1 Geometrical Properties of a Thin Walled Torus

The geometry of the middle surface of the toroidal shell can be parameterised as:

$$\mathbf{r}(\alpha_1, \alpha_2) = \begin{bmatrix} \left(R + r\cos\left(\frac{\alpha_2}{r}\right)\right)\cos\left(\frac{\alpha_1}{R}\right) \\ \left(R + r\cos\left(\frac{\alpha_2}{r}\right)\right)\sin\left(\frac{\alpha_1}{R}\right) \\ r\sin\left(\frac{\alpha_2}{r}\right) \end{bmatrix} \tag{4.7}$$

From this parametrisation the Lamé parameters can be determined from (2.6):

$$A_1(\alpha_1, \alpha_2) = \sqrt{\left(\frac{\partial x}{\partial \alpha_1}\right)^2 + \left(\frac{\partial y}{\partial \alpha_1}\right)^2 + \left(\frac{\partial z}{\partial \alpha_1}\right)^2} = \tag{4.8}$$

$$= \sqrt{\left(-\frac{1}{R}\left(R + r\cos\left(\frac{\alpha_2}{r}\right)\right)\sin\left(\frac{\alpha_1}{R}\right)\right)^2 + \left(\frac{1}{R}\left(R + r\cos\left(\frac{\alpha_2}{r}\right)\right)\cos\left(\frac{\alpha_1}{R}\right)\right)^2} =$$

$$= \frac{1}{R}\left(R + r\cos\left(\frac{\alpha_2}{r}\right)\right)$$

$$\Downarrow$$

$$A_1(\theta) = 1 + \epsilon\cos(\theta) \tag{4.9}$$

Here the two substitutions must be emphasised (cf. figure 4.1):

$$\epsilon = \frac{r}{R} \qquad \text{and} \qquad \theta = \frac{\alpha_2}{r} \tag{4.10}$$

Later these substitutions will show them self convenient. The other Lamé parameter can be be determined in similar way:

$$A_2(\alpha_1, \alpha_2) = \sqrt{\left(\frac{\partial x}{\partial \alpha_2}\right)^2 + \left(\frac{\partial y}{\partial \alpha_2}\right)^2 + \left(\frac{\partial z}{\partial \alpha_2}\right)^2} = \tag{4.11}$$

$$= \sqrt{\left(-\sin\left(\frac{\alpha_2}{r}\right)\cos\left(\frac{\alpha_1}{r}\right)\right)^2 + \left(\sin\left(\frac{\alpha_2}{r}\right)\sin\left(\frac{\alpha_1}{r}\right)\right)^2 + \cos\left(\frac{\alpha_2}{r}\right)^2}$$

$$\Downarrow$$

$$A_2 = 1 \tag{4.12}$$

The radii of curvature are determined through equations (2.7) to (2.10). Though, with the aim of condensing the extend of this thesis, only the final output from this sequence of equations is presented. Also here the substitutions in (4.10) are employed:

$$R_1(\alpha_1, \alpha_2) = \frac{R + r\cos\left(\frac{\alpha_2}{r}\right)}{\cos\left(\frac{\alpha_2}{r}\right)}$$

$$\Downarrow$$

$$R_1(\theta) = \frac{\frac{r}{\epsilon} + r\cos(\theta)}{\cos(\theta)} \tag{4.13}$$

The other radius of curvature is:

$$R_2 = r \tag{4.14}$$

Which corresponds to what is intuitively plausible.

The consistency between the derived Lamé parameters and radii of curvature can be verified through the Codazzi conditions and the condition of Gauss. These are found as equations (2.11) and (2.12). Along with this it can be recognised that if the limit of $R \to \infty$ is taken then $\epsilon \to 0$. If so, then the Lamé parameters and radii of curvature of the torus all reduce to the Lamé parameters and radii of curvature of the cylinder. Naturally the geometrical interpretation if this is that when the limit of $R \to \infty$ is taken, which corresponds to taking the limit of $\epsilon \to 0$, then the torus is straighten and thus approaching the geometry of the cylinder. This is the first example in this chapter of how the results obtained for the cylinder serves as a limiting case of the torus.

4.2 Deformations of the Middle Surface of the Torus

The derived Lamé parameters and radii of curvature are used to determine the deformations of the middle surface of the toroidal shell. Remembering that due to (4.10) $\frac{\partial}{\partial \alpha_2} = \frac{\partial \theta}{\partial \alpha_2} \frac{\partial}{\partial \theta} = \frac{1}{r} \frac{\partial}{\partial \theta}$, then the deformations are determined from equations (2.13):

$$\varepsilon_1 = \frac{1}{r \, (1 + \epsilon \cos{(\theta)})} \left(\frac{\partial u}{\partial \alpha_1} - \epsilon \cos{(\theta)} \, v + \epsilon \sin{(\theta)} \, w \right)$$

$$\varepsilon_2 = \frac{1}{r} \left(\frac{\partial v}{\partial \theta} + w \right)$$

$$\gamma = \frac{1}{r \, (1 + \epsilon \cos{(\theta)})} \left((1 + \epsilon \cos{(\theta)}) \frac{\partial u}{\partial \theta} + \epsilon \sin{(\theta)} \, u + r \frac{\partial v}{\partial \alpha_1} \right)$$

$$\kappa_1 = \frac{1}{r^2 \, (1 + \epsilon \cos{(\theta)})^2} \left(\epsilon r \cos{(\theta)} \frac{\partial u}{\partial \alpha_1} - r^2 \frac{\partial^2 w}{\partial^2 \alpha_1} \right) +$$

$$+ \frac{1}{r \, (1 + \epsilon \cos{(\theta)})} \left(-\frac{\epsilon \sin{(\theta)}}{r} v + \frac{\epsilon \sin{(\theta)}}{r} \frac{\partial w}{\partial \theta} \right) \tag{4.15}$$

$$\kappa_2 = \frac{1}{r^2} \left(\frac{\partial v}{\partial \alpha_2} - \frac{\partial^2 w}{\partial \alpha_2^2} \right)$$

$$\tau = \frac{1}{r^2 \, (1 + \epsilon \cos{(\theta)})^2} \left(\epsilon^2 \cos{(\theta)} \sin{(\theta)} \, u - \epsilon r \sin{(\theta)} \frac{\partial w}{\partial \alpha_1} \right) +$$

$$+ \frac{1}{r \, (1 + \epsilon \cos{(\theta)})} \left(\frac{\epsilon \cos{(\theta)}}{r} \frac{\partial u}{\partial \theta} + \frac{\partial v}{\partial \alpha_1} - \frac{\partial^2 w}{\partial \alpha_1 \theta} \right)$$

Also in these equations it is possible to recover the corresponding relations for the cylinder by taking the limit $\epsilon \to 0$.

4.3 Equilibrium Equations of an Element of the Toroidal Shell

The equations of equilibrium for an infinitesimal element of the toroidal shell are derived from the equations in (2.15) where the normal shearing forces are determined from the first two equations in (2.16). The corresponding equations for the cylinder shell where possible to present explicitly within the format of this thesis. This where possible, because both the Lamé parameters and the radii of curvature are constant and are thus vanishing when differentiating these with respect to the curvilinear coordinates. But in this case A_1 and R_1 are both functions of θ and the differentiations will thus results in a significant increase in number of terms. As mentioned in the introduction to this chapter the mathematical software tool Mathematica® by *Wolfram Research* has been facilitating these calculations. This makes it possible to eliminate the forces and moments in the equilibrium equations by the relations in (2.19) and then eliminate the deformations by inserting the relations presented in previous section. The inertia forces due to the free vibration is of same form as in the cylinder case, which is found as equations (3.14). Through these substitutions a set of three differential equations, formulated in the displacements of the middle surface of the toroidal shell, are obtained.

4.4 Solving the Equations of Equilibrium of the Toroidal Shell

The solution method for the derived equilibrium equations has been discussed in the beginning of the chapter as Galerkin's method. After a trial solution has been substituted into the governing equations this method requires integration over the volume of the continuum under consideration, i.e. with respect to the coordinate variables. But if e.g. one of the trial solutions in (4.2) or (4.4) is inserted into the governing equations and each term of the equations are also divided with the exponential functions of the trial solution, then the only remaining coordinate dependency in the now algebraic equations, is on θ. Thus the integration through the thickness or along the axial direction of the torus is not needed. This simplification falls back on the fact that the Lamé parameters and the radii of curvature of the torus are only functions of θ.

In the meantime the term $(1 + \epsilon \cos(\theta))^{-m}$ can be recognised with different powers of m in the relations in (4.15). This term also arise when A_1 from (4.9) is substituted into the equilibrium equations in (2.15) and (2.16). This term complicates the symbolic integration with respect θ. To get through with the integration this term has instead been approximated by a truncated Taylor expansion. For any torus it is known that $0 < \epsilon < 1$. But in the later application of the torus model it is expectable that ϵ will be small or at least $\epsilon << \frac{1}{2}$. Because of that $\epsilon \cos(\theta)$ will also be small. This makes it relevant simply to regard $\epsilon \cos(\theta)$ as one fictive variable and then with the origin at $\epsilon \cos(\theta) = 0$ expand with respect to this:

$$\frac{1}{(1 + \epsilon \cos(\theta))^m} \simeq \sum_{i=0}^{n} \frac{1}{i!} \left. \frac{\partial^i \left((1+x)^{-m}\right)}{\partial x^i} \right|_{x=0} \epsilon^i \cos(\theta)^i = \tag{4.16}$$

$$= 1 - m\epsilon \cos(\theta) + \frac{m(m+1)}{2} \epsilon^2 \cos(\theta)^2 + ... + \frac{(-1)^n}{n!} \prod_{i=0}^{n} (m+i-1) \epsilon^n \cos(\theta)^n \tag{4.17}$$

where: n Order of Taylor expansion.

By substituting $(1 + \epsilon \cos(\theta))^{-m}$ with this series expansion the equilibrium equations will appear as polynomials in different powers and combinations of $\cos(\theta)$ and $\sin(\theta)$ which are straight forward, though cumbersome, to integrate.

In accordance to Galerkin's method the trial solution related to out-off-plane bending is then formulated in fashion of base functions as (cf. equations (4.5) and (4.2)):

$$\widetilde{\mathbf{u}}_{oop,1} = \left(\mathbf{u}_{oop,0}\boldsymbol{\phi}_{oop,0} + \mathbf{u}_{oop,1}\boldsymbol{\phi}_{oop,1}\right)\mathrm{Re}\left\{e^{\frac{k\alpha_1}{r}}e^{\frac{i\omega c_0 t}{r}}\right\} = \tag{4.18}$$

$$= \left(\begin{bmatrix} u_0 \\ v_0 \\ w_0 \end{bmatrix}\begin{bmatrix} 1 \\ 1 \\ 1 \end{bmatrix} + \begin{bmatrix} u_1 \\ v_1 \\ w_1 \end{bmatrix}\begin{bmatrix} \sin(\theta) \\ \cos(\theta) \\ \sin(\theta) \end{bmatrix}\right)\mathrm{Re}\left\{e^{\frac{k\alpha_1}{r}}e^{\frac{i\omega c_0 t}{r}}\right\} \tag{4.19}$$

And regarding the equations of equilibrium as a differential operator, $\mathbf{L}$, acting on the trial solution the following two integrations must be performed (cf. equation (4.6)):

$$\int_0^{2\pi} \mathbf{L}\widetilde{\mathbf{u}}_{oop,1}\boldsymbol{\phi}_{oop,0}d\theta \quad \text{and} \quad \int_0^{2\pi} \mathbf{L}\widetilde{\mathbf{u}}_{oop,1}\boldsymbol{\phi}_{oop,1}d\theta \tag{4.20}$$

This gives six equations and each equation generally contains all the constant $[u_0\,v_0\,w_0\,u_1\,v_1\,w_1]^T$. By extracting the coefficient multiplied on each of these individual constants, in each of the six equations, a matrix vector equation can be arranged as:

$$\mathbf{M}_{6\times6}\begin{bmatrix} u_0 \\ v_0 \\ w_0 \\ u_1 \\ v_1 \\ w_1 \end{bmatrix} = \mathbf{0} \tag{4.21}$$

From here the remaining steps leading to dispersions curves are identical to what is present in the cylinder case. The corresponding equations for in-plane bending are obtained by simply interchanging sin and cos in $\boldsymbol{\phi}_{oop,1}$ resulting in $\boldsymbol{\phi}_{ip,1}$.

4.5 Correlation Between the Toroidal Shell and Curved Beam Theory

As described previously a Mathematica script has been developed to derive the equilibrium equations for the toroidal shell and to determine dispersion curves related to a given trial solution. Because the model involves the Taylor expansion found in equation (4.17) a sufficient order of this expansion is needed. In appendix A on page 45 a sequence of dispersion plots are found where the trial solution for in-plane bending has been enforced. In accordance to this appendix it is probable that within the interval $0 < \epsilon < \frac{1}{10}$ an order of the Taylor expansion as high as seven is needed to obtain converged results. Naturally, in that connection, it has been ascertained that even higher orders of the Taylor expansion is needed when $\epsilon > \frac{1}{10}$. Identical observations are found for the trial solution for out-off-plane bending. For the time being no further convergence test has been imposed. Instead the validity of the model has been tested by comparing with classical beam theory for both straight beams and curved beams. In figure 4.2 the dispersion curves for the toroidal shell are compared to dispersion curves obtained through curved beam theory. The governing equations of curved beam theory are not presented in this thesis, but can be found in the paper by A. Søe-Knudsen [2010]. In this comparison the order of the Taylor expansion is seven while the trial solution imposed to the model corresponds to
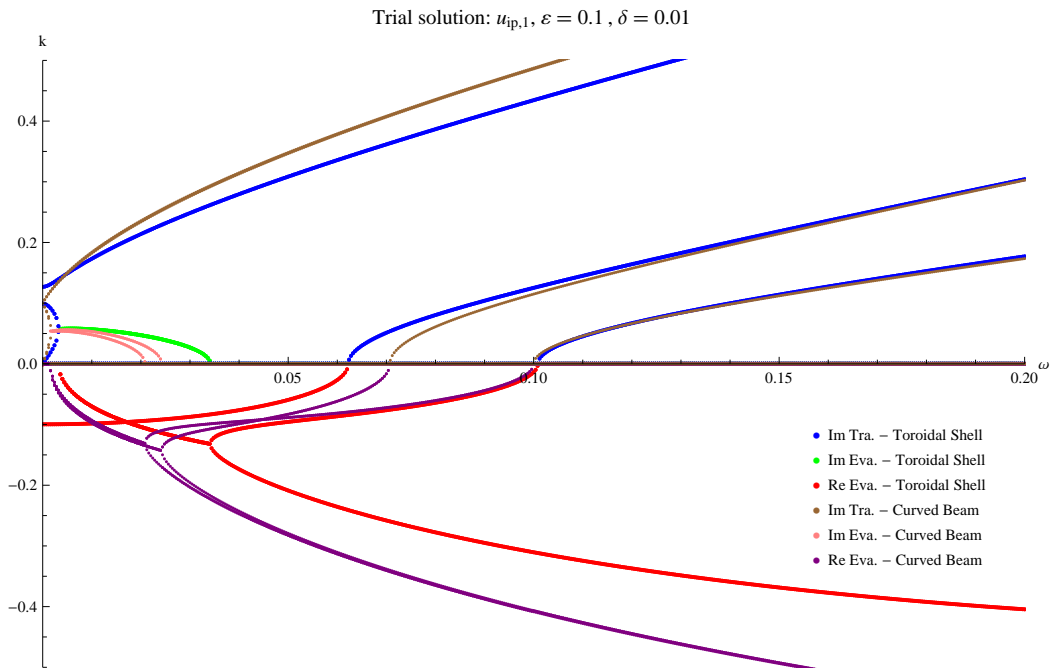
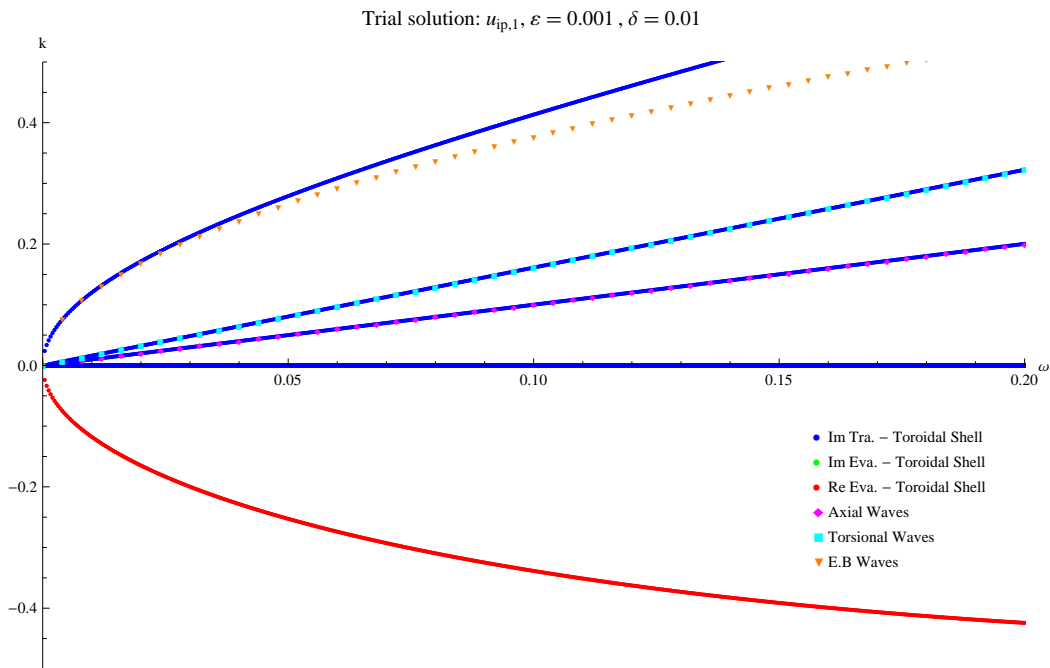**Figure 4.2:** *Dispersion curves for in-plane bending of the the toroidal shell compared to dispersion curves obtained from curved beam theory.*

in-plane bending found in equation (4.4). The values of ϵ and δ are given in the headline of the figure. Except for one of the branches, which will be comment later, the qualitative correlation is clear, and even though this is a comparison between a thin shell and a solid beam a rather close quantitative correlation is also present. It would then be intuitively evident that a

Figure 4.3: *Dispersion curves for in-plane bending of the the toroidal shell compared to dispersion curves obtained from classical straight beam theory.*

thicker shell would show even better quantitative correlation. If the ratio of the thickness-to the radius is increased, the stiffness of the cross section of the torus will naturally also increase. Intuitively this must drag the properties of the toroidal shell in direction of the properties of the solid curved beam, and consequently oppress the additional degrees of freedom that characterise a shell. This expectation can also emerge from the fact that the kinematic constraint on the thin shell theory is that a line perpendicular to the middle surface remain straight and rotates with the middle surface. If the shell is thick this is not fare from the kinematic constraint in the beam theory where the entire cross section of the beam is forced to remain plane and rotate with the centre line. But in this case it turns out that with the present trial solution the dispersion plots are insensitive to the thickness of the shell.

In figure 4.3 dispersion curves from same shell model are plotted. But here $\epsilon = \frac{1}{1000}$ and thus they are compared to results from classical straight beam theory. Also here a close correlation is found. Returning to figure 4.2 and to the branch of which the two models no not agree. It can be seen that the branch belonging to the shell model and cutting on at $\omega \simeq 0.061$ do not interact with any of the other branches. This is not the case for the corresponding branch belonging to the beam model. But when comparing to figure 4.3 it can be seen that this branch corresponds to torsional vibration. As discussed previously torsion is, with respect to a line between $\theta = 0$ and $\theta = \pi$, antisymmetric while the remaining circumferential modes covered by the trial function are symmetric. And as also mentioned anti-symmetric and symmetric circumferential modes do not interact, and thus this is not regarded as a flaw to the shell model.

4.5.1 Higher Order Trial Solutions

The two figures presented above indicate that the derived equilibrium equations are valid. But in the mean time a closer look at the equilibrium equations insinuate that the enforced trial solution, in this case the trial solution for in-plane bending, do not cover the full displacement pattern of the intended vibration mode. Off cause it is self-evident that the trail solution is insufficient in comparison to the general solution given in equation (3.1) on page 15. But as discussed in the beginning of this chapter it is intuitively expectable that the presented trial solutions are sufficient for the two fundamental modes of, respectively, in-plane bending and out-off-plane bending.

As mentioned previously the derived equilibrium equations appear as polynomials in different powers and combinations of $\cos(\theta)$ and $\sin(\theta)$. As an example a term like $\cos(\theta)^2$ can be found in the equilibrium equations. In accordance to Galerkin's method this term is integrated with respect to θ. Thus this term gives:

$$\int \cos(\theta)^2 \, d\theta = \tfrac{1}{4} \sin(2\theta) + \ldots \tag{4.22}$$

But $\sin(2\theta)$ will also enter into the equations if the next term of the general solution where included in the trial solution. This shows that contributions from higher circumferential mode numbers will appear in the equations even though they are not included in the trial solution – contributions which do not necessary vanish when the limes of $0 \le \theta \le 2\pi$ are evaluated after the integration. Thus it is found relevant to investigate the influence of including terms of higher circumferential mode number than what is present in the former trial solutions. First the trail solution for in-plane bending is extended with the term of $m = 2$:

$$\widetilde{\mathbf{u}}_{ip,2} = \left(\begin{bmatrix} u_0 \\ v_0 \\ w_0 \end{bmatrix} + \begin{bmatrix} u_1 \\ v_1 \\ w_1 \end{bmatrix} \begin{bmatrix} \cos(\theta) \\ \sin(\theta) \\ \cos(\theta) \end{bmatrix} + \begin{bmatrix} u_2 \\ v_2 \\ w_2 \end{bmatrix} \begin{bmatrix} \cos(2\theta) \\ \sin(2\theta) \\ \cos(2\theta) \end{bmatrix} \right) \mathrm{Re} \left\{ e^{\frac{k\alpha_1}{r}} e^{\frac{i\omega c_0 t}{r}} \right\} \tag{4.23}$$
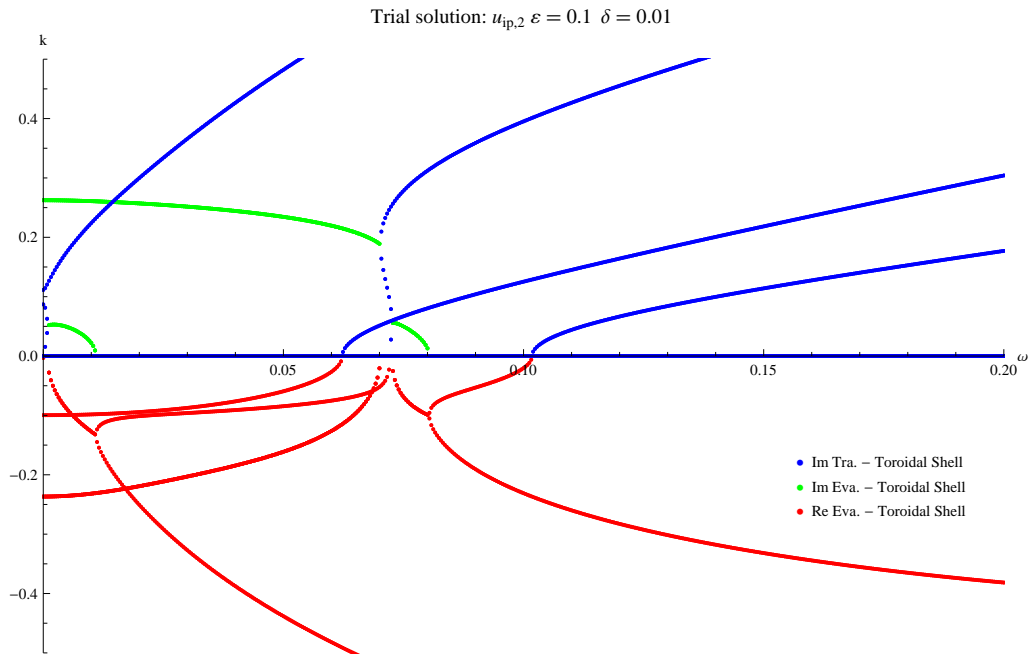
Trial solution: $u_{ip,2}$ $\varepsilon = 0.1$ $\delta = 0.01$

Figure 4.4: *Dispersion curves for the toroidal shell with $\widetilde{\mathbf{u}}_{ip,2}$ as trial solution.*

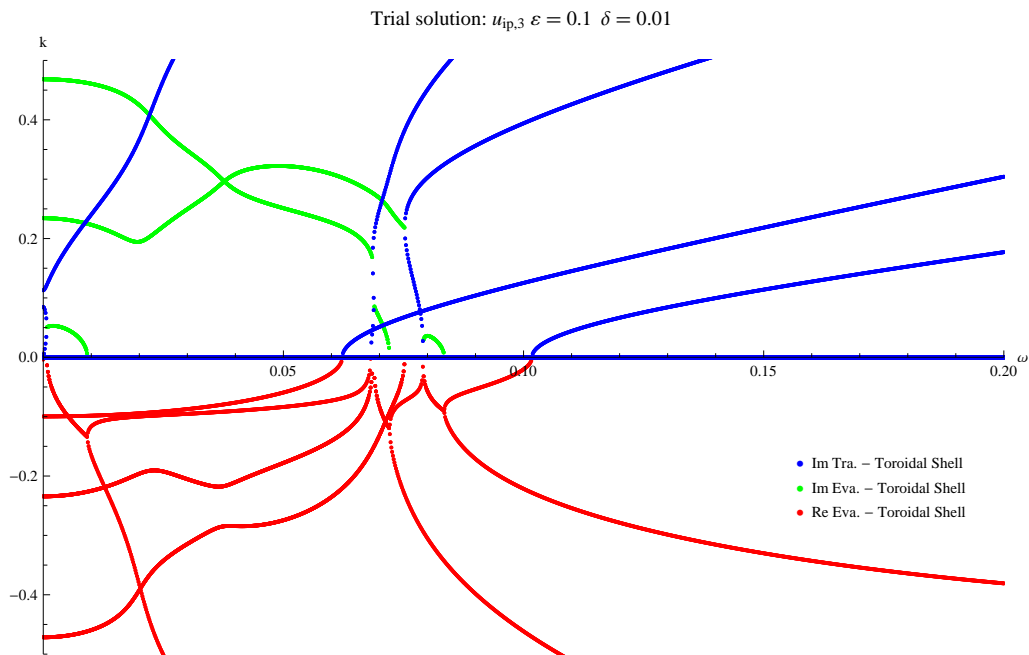Trial solution: $u_{ip,3}$ $\varepsilon = 0.1$ $\delta = 0.01$

Figure 4.5: *Dispersion curves for the toroidal shell with $\widetilde{\mathbf{u}}_{ip,3}$ as trial solution.*

This increases the number of unknowns with three, but it also introduces a vector of three new base functions. So after applying Galerkin's method the problem consists of nine equations and nine unknown. In figure 4.4 a dispersion plot related to this trail solution is seen. Obviously this differs from the dispersion plot in figure 4.2 even though the only difference is the extra term in the trial solution. The difference is not only the introduction of a new set of branches but also some of the branches which are present in both dispersion plots differ. The new branches are examples of the additional degrees of freedom which are not present in beam theory, but characterises a shell. They will not be investigated further in this thesis, so at this stage it can just be

observed that they exists, and that they to some extend interrupt the clarity of the fundamental branches.

Following along same path the trial solution is also extended with the term corresponding to $m = 3$:

$$\widetilde{\mathbf{u}}_{ip,3} = \widetilde{\mathbf{u}}_{ip,2} + \begin{bmatrix} u_3 \\ v_3 \\ w_3 \end{bmatrix} \begin{bmatrix} \cos(3\theta) \\ \sin(3\theta) \\ \cos(3\theta) \end{bmatrix} \mathrm{Re}\left\{ e^{\frac{k\alpha_1}{r}} e^{\frac{i\omega c_0 t}{r}} \right\} \tag{4.24}$$

The dispersion curve corresponding to this trial solution is seen in figure 4.5. Again, with this trial solution the branches which are common to the previous plots are affected. Now, if the thickness of the shell is increased to the limit of the thin shell theory, i.e. $\delta = \frac{1}{20}$ cf. section 2.1 on page 5, then the dispersion plots starts to correlate closely. In figure 4.6 these two dispersion plots are plotted in same figure. Like with the Taylor expansion involved in the derivation of the equilibrium equations, this indicates that the results start to converge when an appropriate number of term are included in the trail solution. In appendix A the dispersion curves related to $\widetilde{\mathbf{u}}_{ip,2}$ and $\widetilde{\mathbf{u}}_{ip,3}$ are shown where $\epsilon = \frac{1}{1000}$. The two curves are here compared to the results of straight beams and the only visible difference is the additional branches due to the introduction of, respectively, $m = 2$ and $m = 3$.
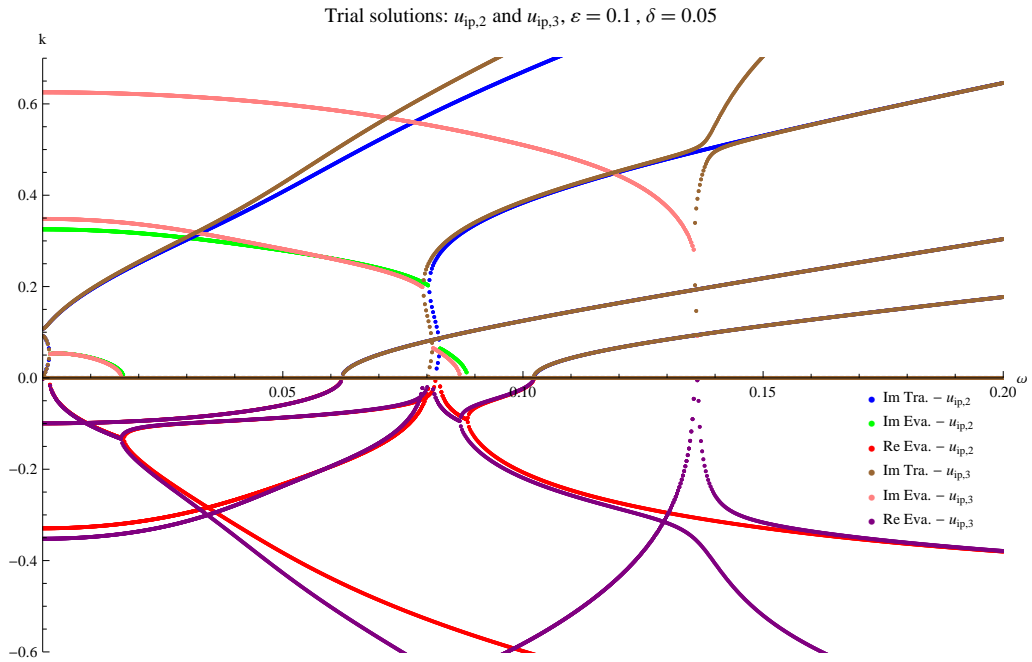
Figure 4.6: *Comparison between the dispersion curves related to, respectively, $\widetilde{\mathbf{u}}_{ip,2}$ and $\widetilde{\mathbf{u}}_{ip,3}$ when $\delta = \frac{1}{20}$.*

Unfortunately it has not been possible to further extend the trial solution and then let Mathematica expand the determinant. With the trial solution in (4.24) the system of equations, after imposing Galerkin's method, consists of 12 very cumbersome equations and 12 unknowns. When Mathematica then is asked to expand the determinant it runs into some unexplained error. But in the mean time a close look at this 12-by-12 matrix reveals that the second column only has a term in second row. This is because the first three columns of the matrix refers to $m = 0$ and the second of these then refers to torsional vibration. Again this falls back on the fact that torsion is antisymmetric while the remaining circumferential modes of the in-plan trial solution are symmetric. Thus second row and column are uncoupled from the rest. This can be illustrated as:

$$
\underset{12\times12}{\mathbf{M}} =
\begin{array}{c}
\\
1\\
2\\
3\\
\vdots\\
12
\end{array}
\begin{array}{cccccc}
1 & 2 & 3 & \ldots & 12 \\
\end{array}
\begin{bmatrix}
\bullet & 0 & \bullet & \ldots & \bullet \\
0 & \bullet & 0 & \ldots & 0 \\
\bullet & 0 & \bullet & \ldots & \bullet \\
\vdots & \vdots & \vdots & \ddots & \bullet \\
0 & 0 & \bullet & \bullet & \bullet
\end{bmatrix}
\tag{4.25}
$$

It makes it possible to determine the determinant of the 12-by-12 matrix by extracting the term at position (2,2) and then multiply this with the determinant of the remaining 11-by-11 minor. In this case Mathematica do not run into errors making it is possible to present the results above. But it shows that the present calculations are at the limit of what Mathematical can handle. Due to this it has not succeeded to extend the trial solution even further and then expand the determinant.

As discussed previously, if the thickness of the shell is increased, then the properties of the toroidal shell are expected to be dragged in direction of the properties of a solid curved beam. Thus, in figure 4.7 a dispersion plot, where $\delta = \frac{1}{9}$, is compared to the curved beam theory. Well aware that this thickness-to-radius ratio is beyond the limitations on the thin shell theory the correlation to the curved beam theory is in this case even better in the low frequency range than what is present in figure 4.2.
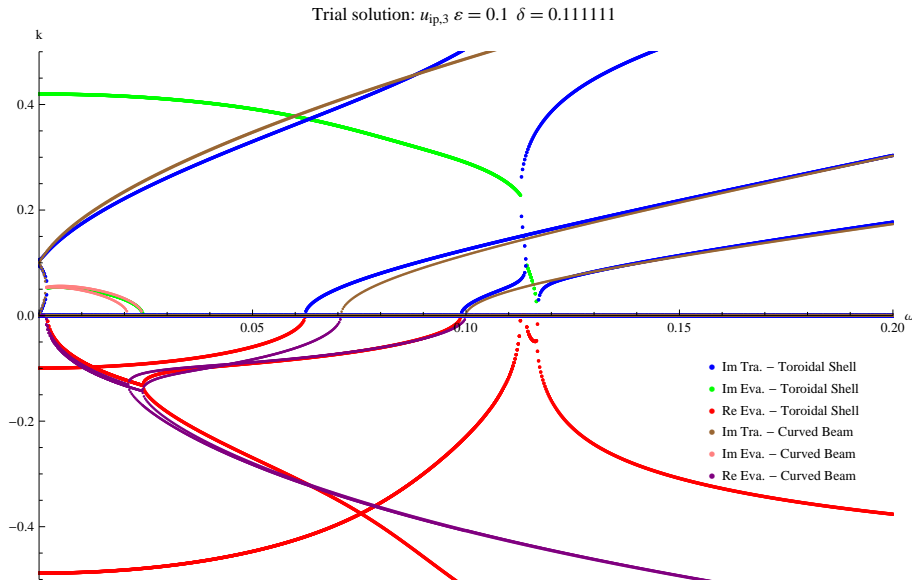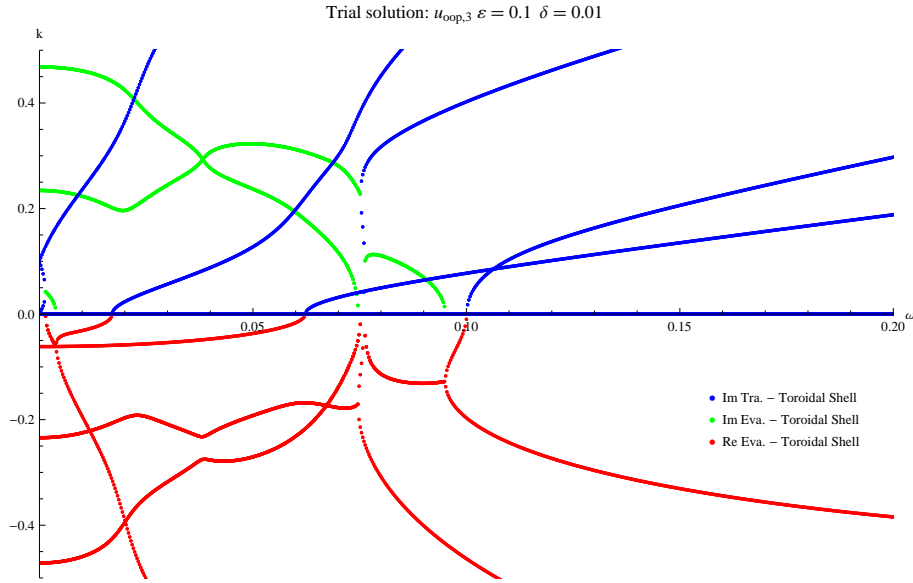

Figure 4.7: *Comparison between the curved beam theory and the toroidal shell with $\widetilde{\mathbf{u}}_{ip,3}$ as the trail solution and $\delta = \frac{1}{9}$.*

Until this stage it has been shown that the nature of the equilibrium equations converge with an increasing the order of the Taylor expansion in equation (4.17). It has been found probable that up to a value of $\epsilon = \frac{1}{10}$ then a seventh order Taylor it sufficient. Having in mind that it has not been possible to extend the trial solution for in-plane bending to cover more than $m = 0, 1, 2, 3$, then the close correlation between the dispersion plots corresponding to $\widetilde{\mathbf{u}}_{ip,2}$ and $\widetilde{\mathbf{u}}_{ip,3}$, at $\delta = \frac{1}{20}$, also indicates convergence with respect to the number of term in the trial solution. Consequently, $\widetilde{\mathbf{u}}_{ip,3}$ is regarded as the best candidate for a valid trial solution for in-plane bending.

As a final topic the dispersion curves related to out-off-plane bending will be presented. Based on the experiences from above the, assumable, best candidate for a trial solution for out-off-plane bending is obtained by interchanging sin and cos in $\widetilde{\mathbf{u}}_{ip,3}$. Thus:

$$\widetilde{\mathbf{u}}_{oop,3} = \left(\begin{bmatrix} u_0 \\ v_0 \\ w_0 \end{bmatrix} + \sum_{m=1}^{3} \begin{bmatrix} u_m \\ v_m \\ w_m \end{bmatrix} \begin{bmatrix} \sin{(m\theta)} \\ \cos{(m\theta)} \\ \sin{(m\theta)} \end{bmatrix} \right) \mathrm{Re} \left\{ e^{\frac{k\alpha_1}{r}} e^{\frac{i\omega c_0 t}{r}} \right\} \tag{4.26}$$

Figure 4.8: *Comparison between the curved beam theory and the toroidal shell with $\widetilde{\mathbf{u}}_{oop,3}$ as the trail solution and $\delta = \frac{1}{100}$.*
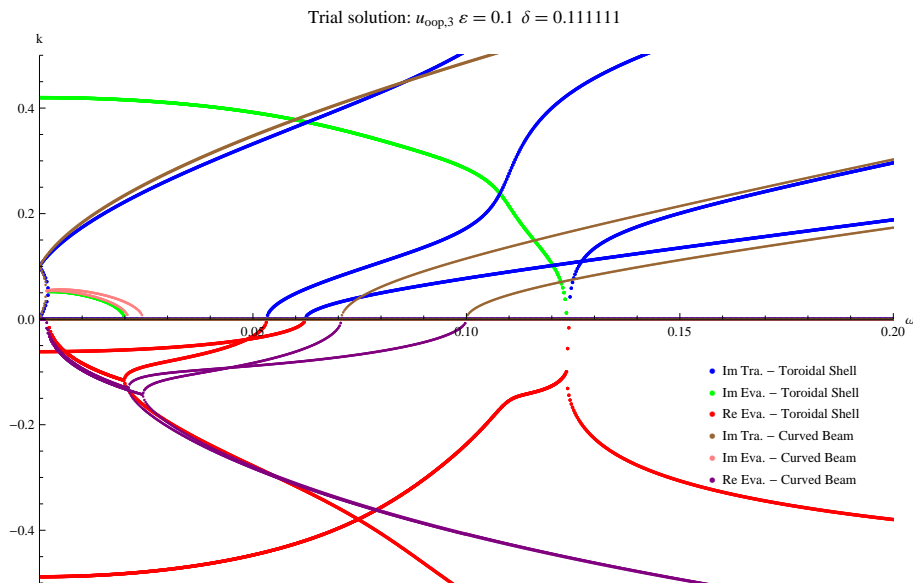
Figure 4.9: *Comparison between the curved beam theory and the toroidal shell with $\widetilde{\mathbf{u}}_{oop,3}$ as the trail solution and $\delta = \frac{1}{9}$.*

First the dispersion plot at $\delta = \frac{1}{100}$ is seen in figure 4.8. From this it can be seen that the branch corresponding to axial vibration do not interact with the other branches. This is because this

mode is symmetric will the remaining modes are antisymmetric. In figure 4.9 the thickness-to-radius ratio has been increased to $\delta = \frac{1}{9}$ and then compared to results from curved beam theory. Like in figure 4.7 this also shows a close correlation in the low frequency range.

Chapter

5

Discussions, Conclusions, & Future Perspectives

In this thesis a shell model of a thin walled infinite cylinder has be established. From this model the dynamical properties has been extracted in fashion of dispersion curves. These dispersion curves have been compared to corresponding results obtained through classical Bernoulli-Euler beam theory. The comparison has revealed a close correlation on the simplest vibration modes for this geometry. With this point of reference a shell model of a thin walled infinite torus has also been developed. Trial solutions for, respectively, in-plane bending and out-off-plane bending has been formulated and enforced on the model. A system of equally many algebraic equations and unknowns has been established by Galerkin's method and from these equations the dispersion curves related to the enforced trial solutions has been obtained.

The derivation of the equilibrium equations of the toroidal shell involves a Taylor expansion on the parameter ϵ. Even when this parameter is as small as $\frac{1}{10}$ the results show that a rather high ordered expansion is needed to obtain converging results. At $\epsilon = \frac{1}{10}$ the studies also show that for a very thin shell, i.e. for $\delta = \frac{1}{100}$, the two fundamental vibration modes of in-plane bending and out-off-plane bending are not isolated from higher modes. Thereby the intuitive expectation of e.g. regarding the out-off-plane bending as a simple coupling between Bernoulli-Euler bending and torsion only holds at relatively low frequencies and near and outside the limit of the thin shell theory where the shell thickness adds sufficiently stiffness to the cross section. But it is also made probable that, also for thinner shells, the validity of this expectation increases as the torus is straightened out.

From this it can be concluded that the governing differential equations of the toroidal shell, which have been derived, are valid. With an order of seven of the Taylor expansion involved in the differential equations, the dispersion curves have converged with respect to ϵ within the interval $0 < \epsilon < \frac{1}{10}$. At the limit of the thin shell theory, i.e. when $\delta = \frac{1}{20}$, and when $\epsilon = \frac{1}{10}$ it seems likely that the trial solution needs the terms from $m = 0$ to $m = 3$ in order to obtain converging dispersion curves related to the two fundamental modes of, respectively, in-plane bending and out-off-plane bending. But as mentioned it is also seen that the strength of this statement increases as the value of ϵ decreases.

In this thesis the focus and benchmarking has only been on the fundamental vibration modes with the purpose of validating the shell model. Thus the concern with respect to the trial solutions has only been on their ability to attain the dispersion curves related to these fundamental modes. But as long as the importance of higher modes, with respect to the fatigue inducing mechanisms initiating this thesis, are not known, these trail solutions might be insufficient. If higher order modes are in fact important the solution method, due to Galerkin, does not prevent a further extension of the imposed trial solutions. But due to the unexplained error in Mathematica it has not been possible to do so.

5.1 Future Perspectives

From the introduction it is clear that this thesis only is concerned with the first milestone of determining the wave guide properties of flexible pipes like those produced by NKT Flexibles; namely the milestone of determining the waveguide properties of a thin walled pipe having a single bend of constant bending radius. So the existence of possible future work is obvious.

First subject could be to search for any alternative solution method to Galerkin's method. The governing equations of the toroidal shell can generally be recognised as coupled partial differential equations with periodic coefficients. Literature within this particular field of mathematic is available. The *Mathieu function* is known to be the trial solution to a family of these type of differential equations and thus might be helpful, cf. V Krylov [1997] and Weisstein [2011].

When a satisfactory solution method has been found and reliable dispersion curves are determined the relation between the wave number and the frequency can be approximated through asymptotic expansion. Thereby the dominating terms will be extracted from the analytical solution making the relations fare less cumbersome. Until this stage the examined geometry has been of infinite extend. As explained in the introduction the waveguide properties of an infinite geometry can be used to determine the waveguide properties of a bounded geometry through boundary integral equation method. Thus the asymptotic expanded solution to the infinite torus can be used to determine the waveguide properties of only a small section of the torus which correspond to a bend thin walled pipe section.

With respect to the pipes produced by NKT Flexibles at least two relevant advancements could be followed by the model of the wave guide properties of a bend thin walled pipe:

- The load carrying layer of the pipes produced by NKT Flexibles is expected to be close to or outside the limit of the applied shell theory. A relevant advancement is therefore to introduce higher order deformation theory which is cover by thick shell theory.

- The pipes are, in their application, submerged in the sea and they are conveying fluid. Due to this the fluid interaction is relevant to consider. The nature of the fluid interaction inside and outside the pipe wall is fundamentally different. Considering a cross section of the pipe, then the fluid inside the pipe is bounded because the pipe is closed while outside the pipe the fluid is unbounded due to the wide extend of the sea.

A long-range perspective is to extend the thick shell model by incorporation of the anisotropic nature of the pipe wall due to steel armouring. This could might be done by use of the *Stroh formalism* or the *Lekhnitskii formalism*, cf. Ting [1996] or Lekhnitskii [1981, original Russian edition: 1977]. Another long-range perspective is to take the flow of the fluid inside the pipe into consideration and investigate how the flow velocity affects the waveguide properties of the pipe. A final long-termed perspective is to include damping. If the fluid outside the pipe is regarded as infinite, this will off cause act as a energy dissipating mechanism. But damping due to friction and slipping between the different layers in the pipe could also be relevant topics.

Bibliography

S. V. Sorokin A. Søe-Knudsen. Modelling of linear wave propagation in spatial fluid filled pipe systems consisting of elastic curved and straight elements. *Journal of Sound and Vibration*, pages 5116–5146, 2010.

Raymond H. Plaut Akhilesh K. Jha, Daniel J. Inman. Free vibration analysis of an inflated toroidal shell. *Journal of Vibration and Acoustics*, pages 387–397, 2002.

Dr Hugh Goyder, editor. *On the Modelling of Noise Generation in Corrugated Pipes*, 2009. ASME 2009 Pressure Vessels and Piping Division Conference.

Clive L. Dym Irving H. Shames. *Energy and Finite Element Methods in Structural Mechanics*. Taylor & Francis Inc, 1991.

S. G. Lekhnitskii. *Theory of Elasticity of an Anisotropic Body*. Mir Publishers, 1981, original Russian edition: 1977.

Günes Nakiboglu. Whistling behaviour of periodic systems: Corrugated pipes and multiple side branch systems. *International Journal of Mechanical Sciences*, 2010.

V. V. Novozhilov. *The Theory Of Thin Shells*. P. Noordhoff LTD., 1959.

Singiresu S. Rao. *Mechanical Vibrations*. Thomson Canada Limited, 4th edition, 2003.

Martin Raussen. *Elementary Differential Geometry - Curves and Surfaces*. Department of Mathematical Sciences, Aalborg University, 2007.

Lord Rayleigh. *The Theory of Sound*. Republished in 1945 by Dover Publications, 1894.

Sergey V. Sorokin. *Lecture Notes on Machine Acoustics*. 2010.

Stephen P. Timoshenko. *Theory of Plates and Shells*. McGraw-Hill, second international edition edition, 1959.

Thomas C. Ting. *Anisotropic Elasticity: Theory and Applications*. Oxford University Press, 1996.

S V Sorokin V Krylov. Dynamics of elastic beams with controlled distributed stiffness parameters. *IOP Science*, pages 573–582, 1997.

Eric W Weisstein. Mathieu function. *MathWorld – A Wolfram Web Resource*, page http://mathworld.wolfram.com/MathieuFunction.html, 2011.

Appendix

A

Convergence of Torus Model

The dispersion plots in figures A.1 through A.7 illustrate how the results of the toroidal shell model, with the trail solution for in-plane bending given in equation (4.4), stabilise when the order of the Taylor expansion in equation (4.17) increase from first order to seventh order. In these plots $\epsilon = \frac{1}{10}$ while $\delta = \frac{1}{100}$.

Similar plots are found in figures A.8 through A.10 though here $\epsilon = \frac{1}{1000}$. This makes the geometry of the torus almost identical to the cylinder. From the plots it is seen that the results stabilise already with a second order Taylor expansion and that no visible difference is seen between the results obtained with the second order expansion and a seventh order expansion. Similar dispersion plots for the two higher order trial solutions, $\widetilde{\mathbf{u}}_{ip,2}$ and $\widetilde{\mathbf{u}}_{ip,3}$, are seen in figures A.11 and A.12. No difference is found between these two plots except for the additional branch in the second one.
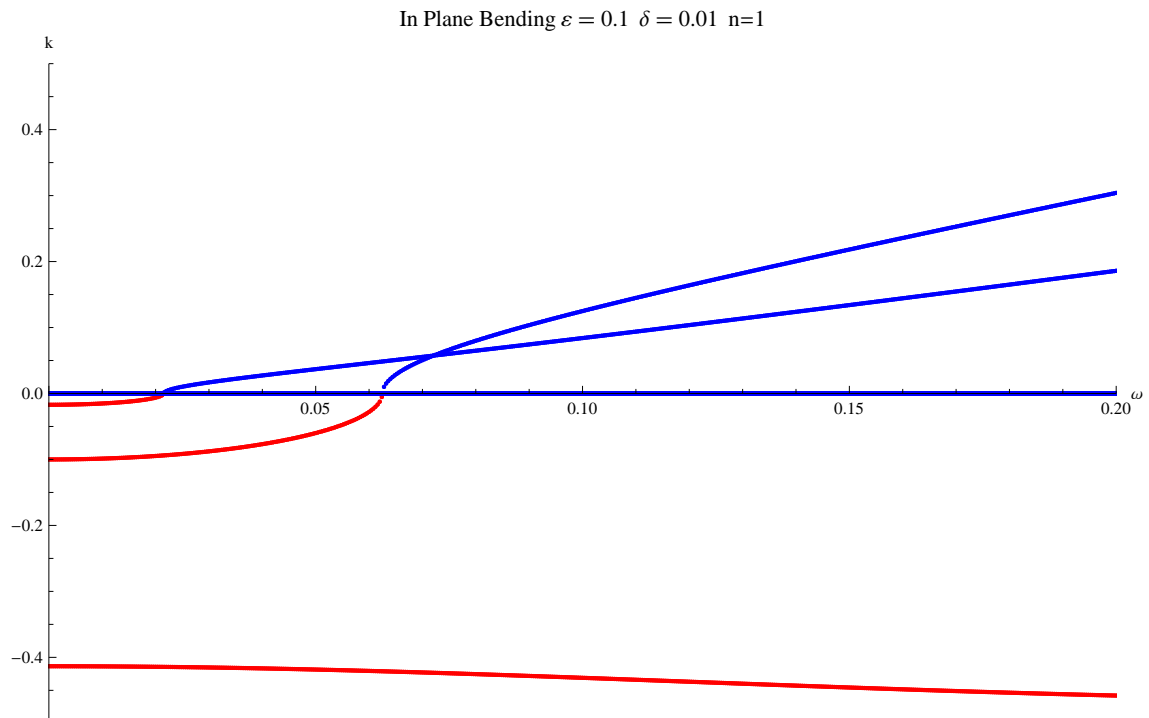
Figure A.1: *Dispersion curves for the toroidal shell.*

In Plane Bending $\varepsilon = 0.1$ $\delta = 0.01$ n=2
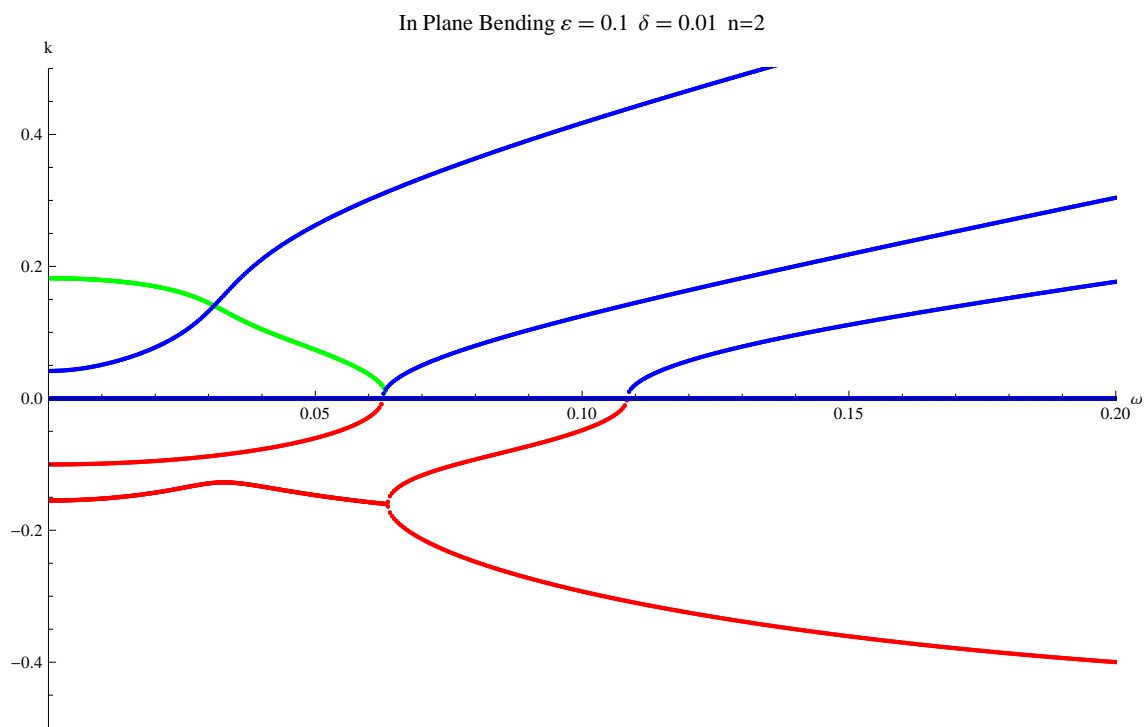
Figure A.2: *Dispersion curves for the toroidal shell.*

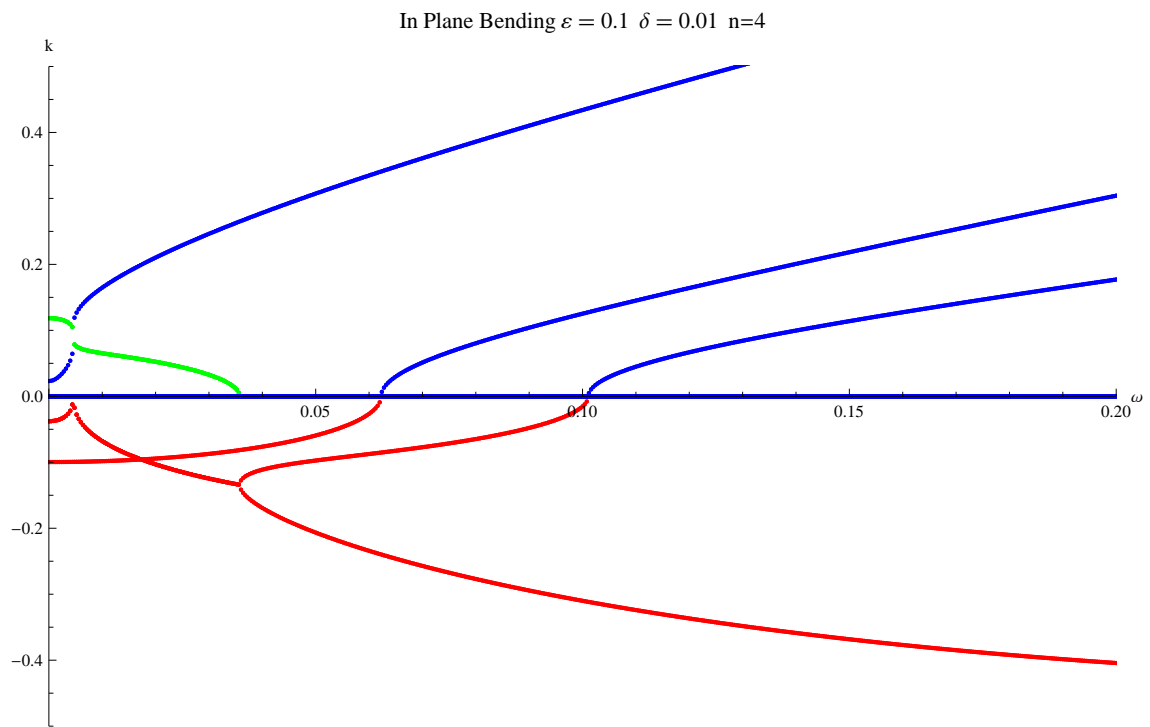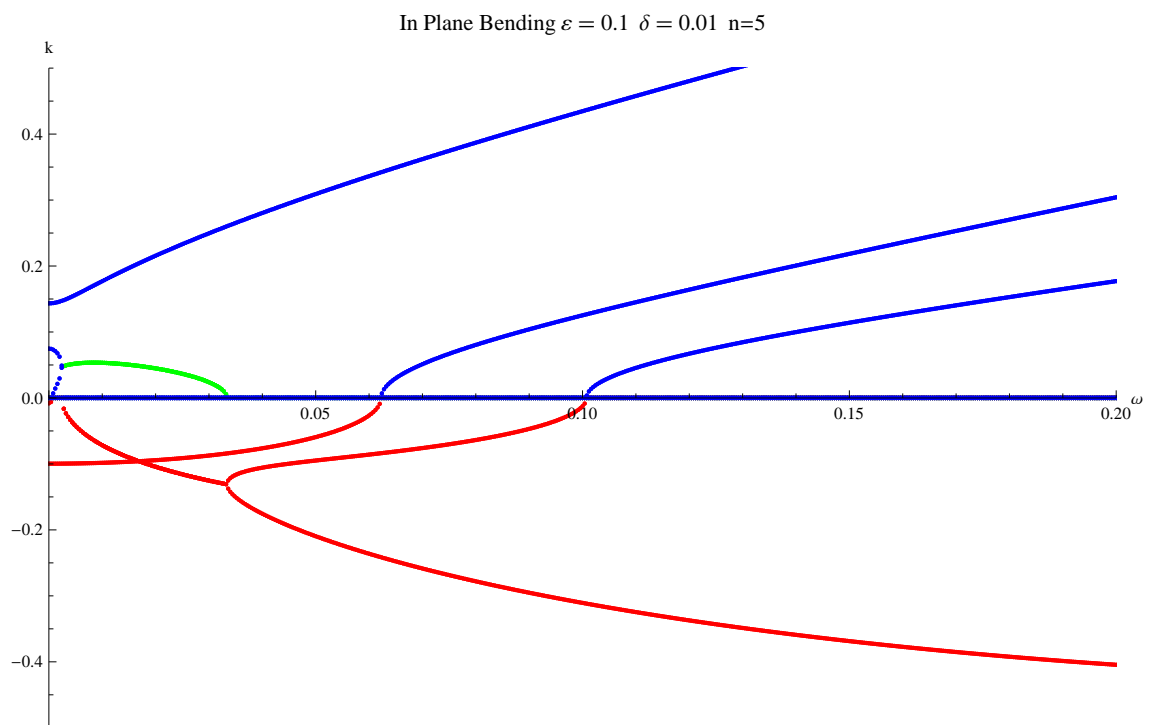In Plane Bending $\varepsilon = 0.1$ $\delta = 0.01$ n=3
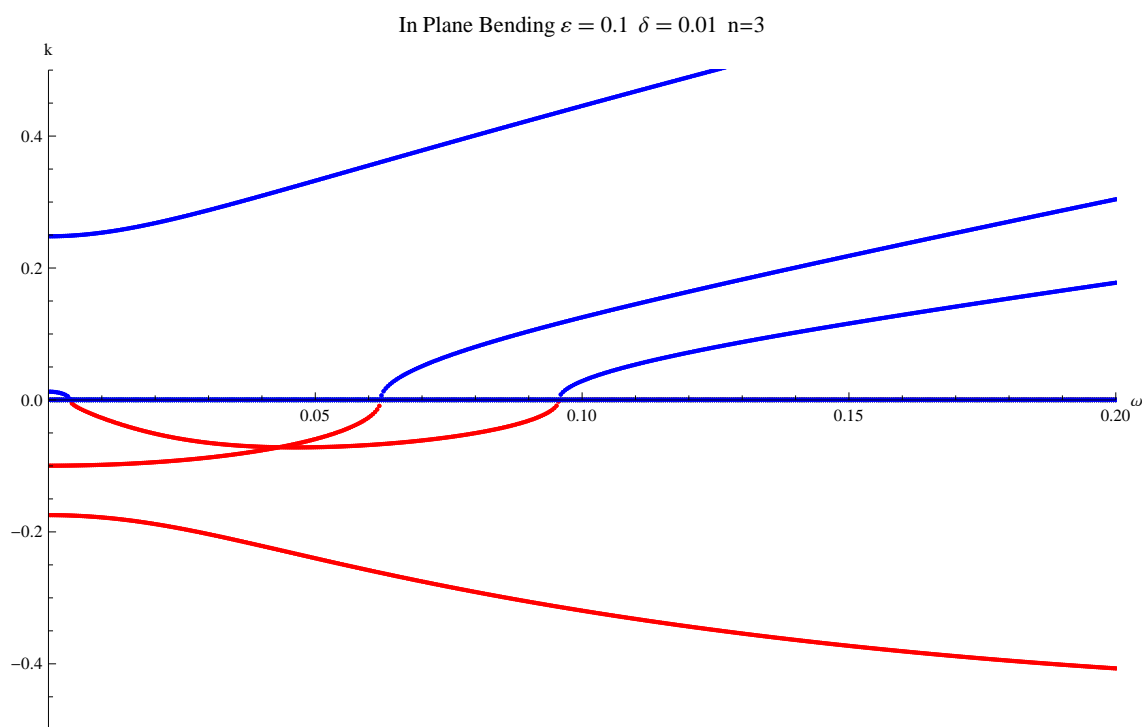
Figure A.3: *Dispersion curves for the toroidal shell.*

Figure A.4: *Dispersion curves for the toroidal shell.*
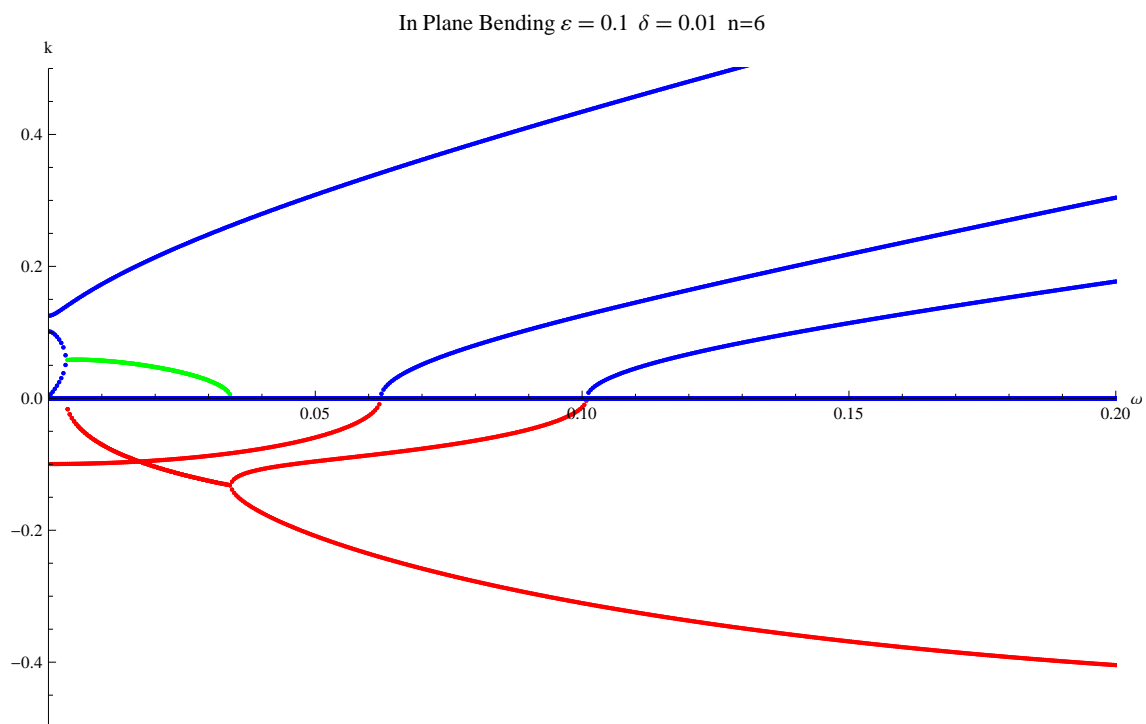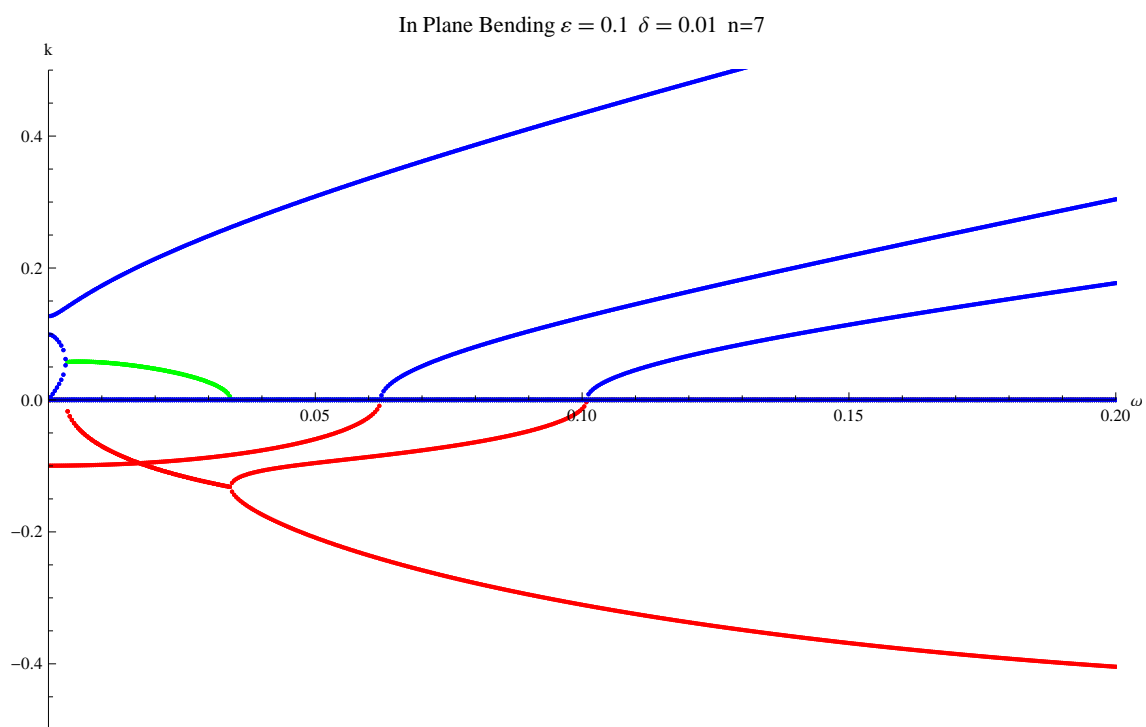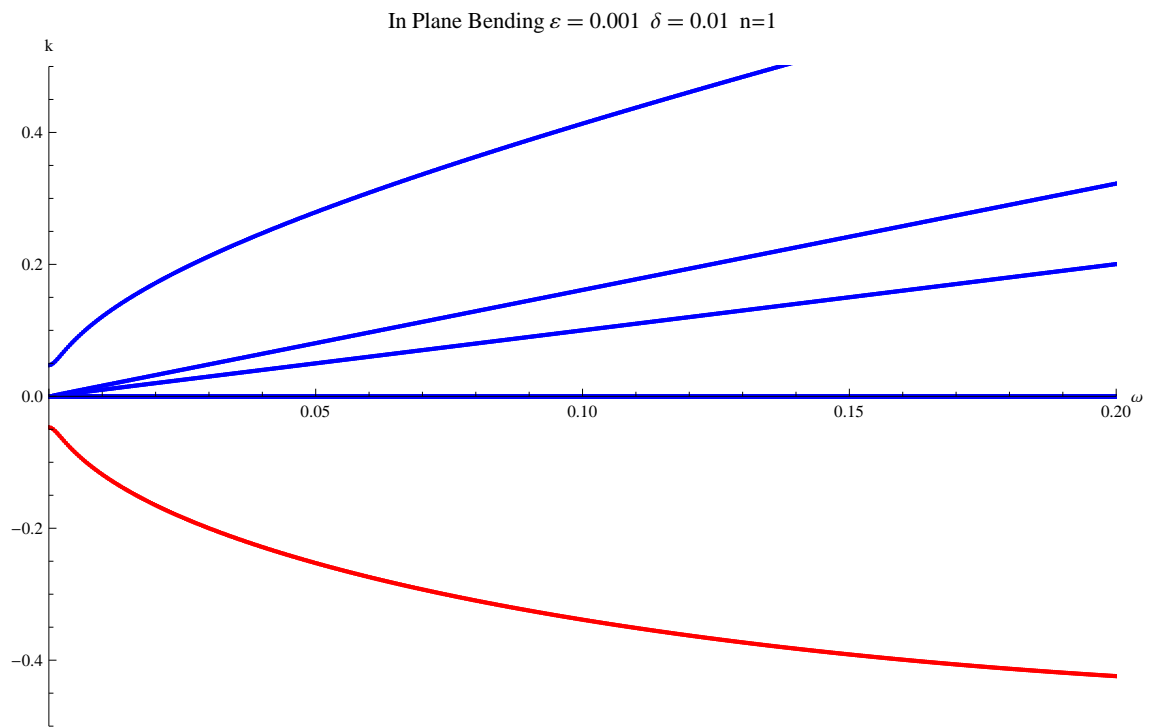

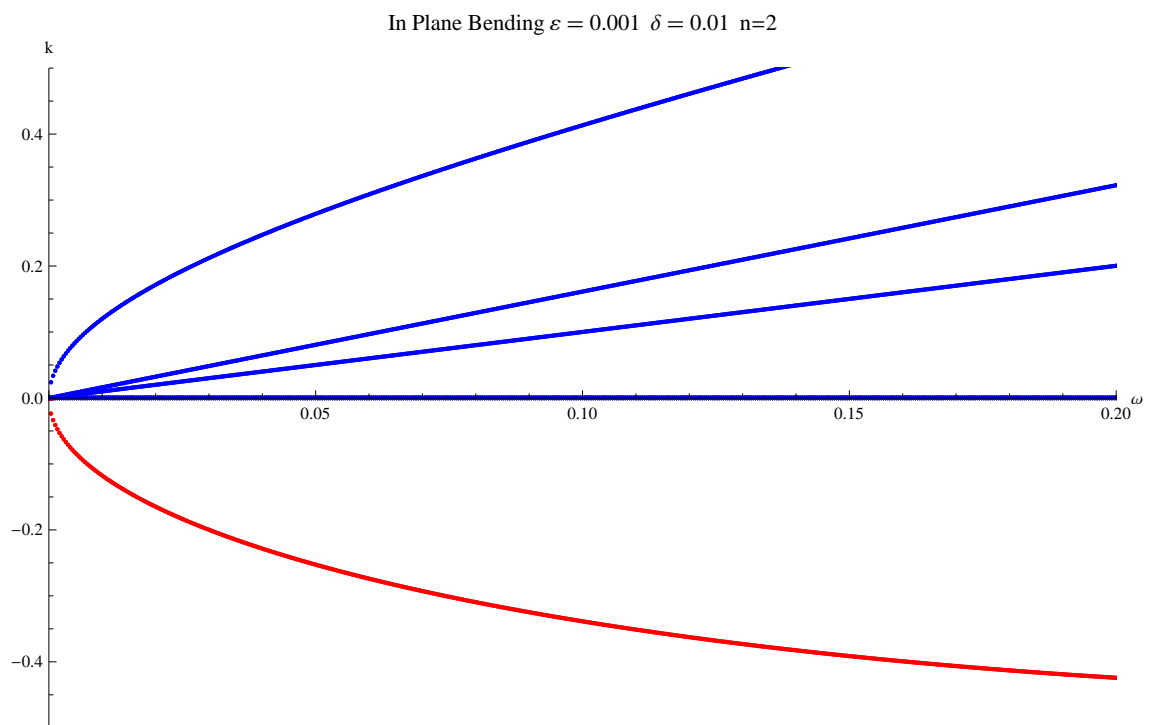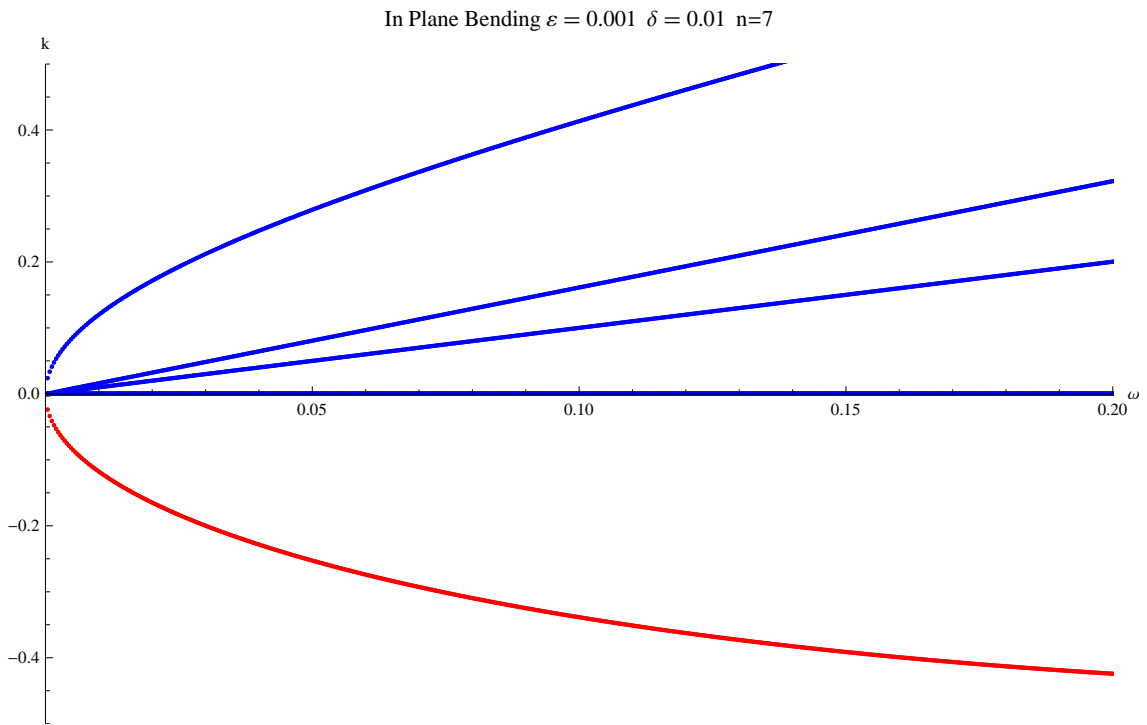**Figure A.5:** *Dispersion curves for the toroidal shell.*

In Plane Bending $\varepsilon = 0.1$ $\delta = 0.01$ n=6

Figure A.6: *Dispersion curves for the toroidal shell.*

In Plane Bending $\varepsilon = 0.1$ $\delta = 0.01$ n=7

Figure A.7: *Dispersion curves for the toroidal shell.*

Figure A.8: *Dispersion curves for the toroidal shell.*

Figure A.9: *Dispersion curves for the toroidal shell.*

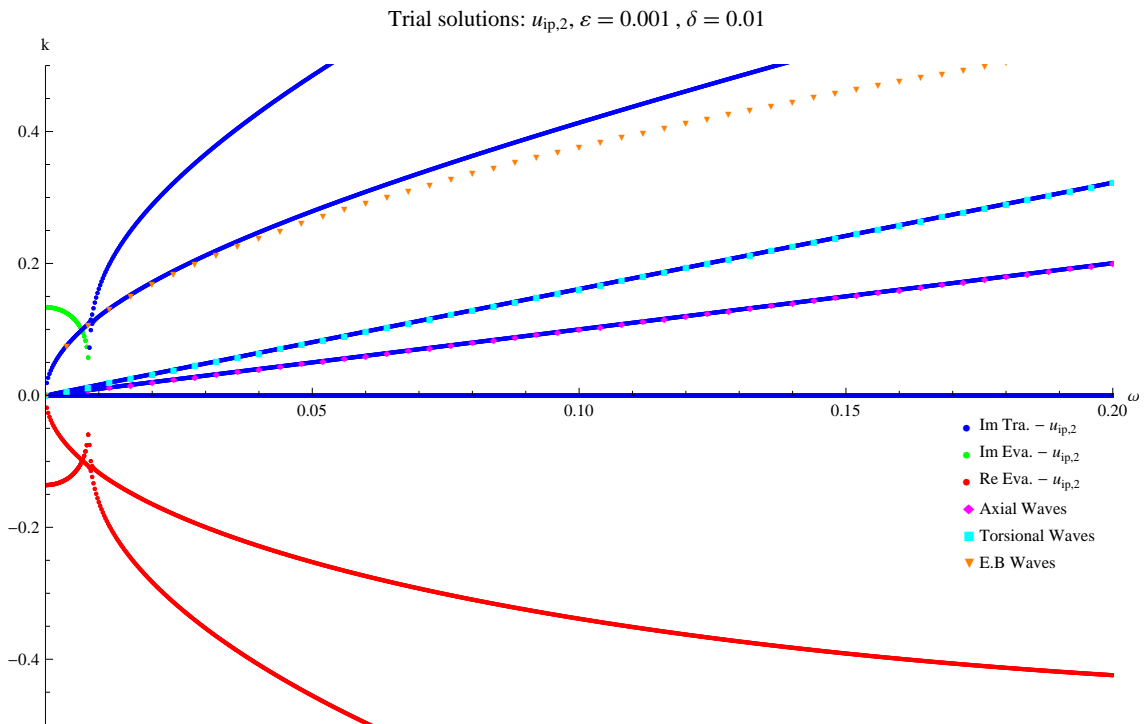**Figure A.10:** *Dispersion curves for the toroidal shell.*
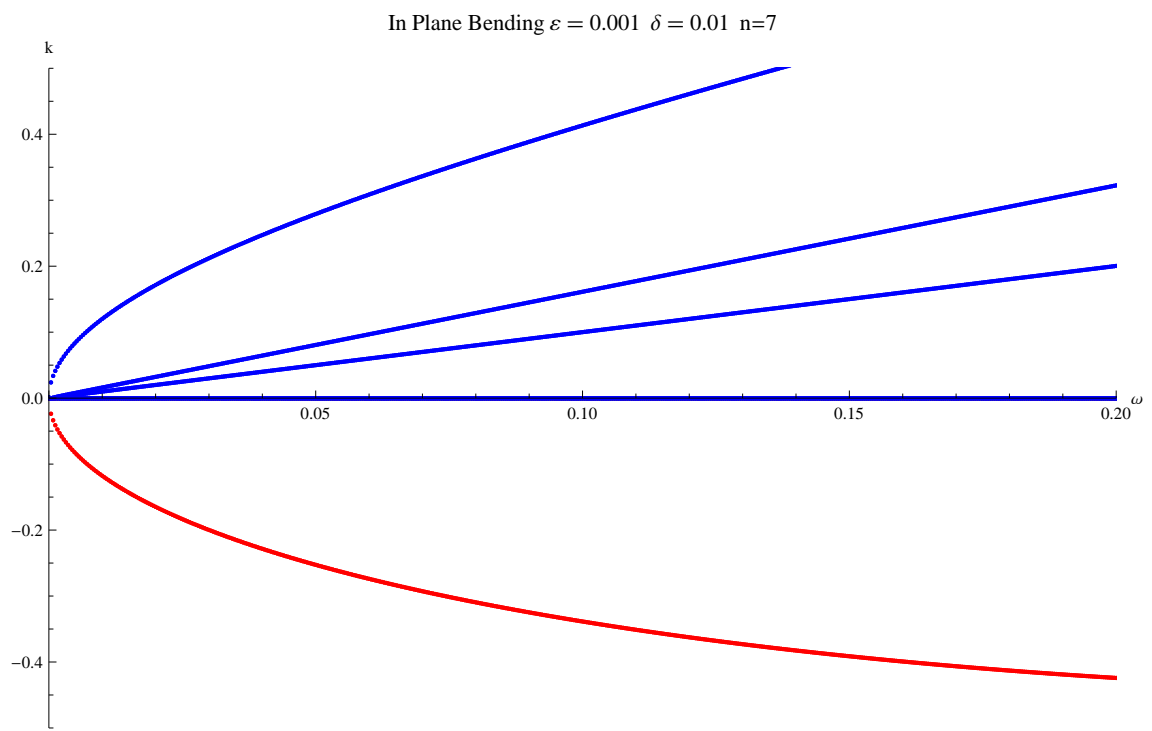

Figure A.11: *Dispersion curves for the toroidal shell.*

Figure A.12: *Dispersion curves for the toroidal shell.*